

**POLITECNICO**  
**MILANO 1863**

The *Sea Harvester*:  
Design of a supersonic anti-ship cruise missile



**Medhelan**

Carminati Luca - 943690

Foletti Nicola – 942538

Lardo Gianluca - 945857

Mascetti Stefano - 940314

Orec Pierre - 962275

Corsi Giulio - 944379

Grusovin Sofia - 940015

Magni Luca - 946362

Nunu Antonio Daniel - 971126

Final Report

Course of Launch System  
School of Industrial Engineering  
Academic Year 2020-2021

## **Abstract**

The purpose of this report is the conceptual design of a supersonic anti-ship cruise missile starting from the requirements of 75 km range, compatibility with the launch platform SH-60, 250 kg warhead, and launch from 1 km altitude with the helicopter moving at 250 km/h.

The first part of the report covers the organization of the project, starting from classical considerations on the conceptual design and choosing the design flow that will be followed through the overall study. To help reducing the complexity of the project, a House of Quality is used in the first phase of the project management. From there, a baseline missile is selected to speed up the early design stages. To conclude this part, a Pareto sensitivity analysis is assessed in order to better understand the principal parameters driving the design.

A detailed description of the conceptual design follows, subdivided in sections for each step of the iterative process. The first step is the prediction of the aerodynamics of the missile, from which then the propulsion is analyzed subdividing it in two parts: the first one about the Ramjet analysis, which results are then used in the second one for the SRM analysis. A similar subdivision is used for the weight evaluation. At this point, the trajectory of the missile is explained, followed by the structural analysis and a Monte Carlo simulation to account for the effects of external wind and mass approximation. Finally, some considerations about aerodynamic stability can be done.

After the conceptual design, a first version of the *Sea Harvester* is proposed, which fulfills all the requirements stated at the beginning with the exception of the warhead mass on which some considerations must be done about the explosive properties and the compatibility with the helicopter.

# Contents

<b>1</b>	<b>Introduction</b>	<b>1</b>
1.1	Mission scenario definition . . . . .	1
<b>2</b>	<b>Project Management</b>	<b>2</b>
2.1	House of Quality . . . . .	3
2.2	Risk analysis . . . . .	4
2.3	Baseline Design . . . . .	5
2.4	Sensitivity analysis . . . . .	6
<b>3</b>	<b>Conceptual design</b>	<b>7</b>
3.1	Aerodynamics . . . . .	7
3.1.1	Predicting missile aerodynamics . . . . .	7
3.1.2	Nose fineness and geometry compromise . . . . .	7
3.1.3	Total drag prediction . . . . .	8
3.1.4	Stabilizers: flare, wings and tails . . . . .	10
3.2	Propulsion . . . . .	10
3.2.1	Propulsion considerations in the missile design . . . . .	11
3.2.2	Ramjet sustain: fuel choice . . . . .	11
3.2.3	Ramjet flight optimization $L = W$ . . . . .	12
3.2.4	Ramjet sustain: supersonic/subsonic inlet integration . . . . .	12
3.2.5	Ramjet sustain: combustion temperature . . . . .	15
3.2.6	Ramjet cruise flight optimization $T = D$ . . . . .	16
3.2.7	Ramjet acceleration flight optimization $T = D + F_{\Delta v}$ . . . . .	16
3.2.8	Aerothermodynamic relations for the combustor . . . . .	16
3.2.9	Ramjet sustain: combustor design considerations . . . . .	17
3.2.10	Ramjet sustain: specific impulse, thrust prediction, and efficiency . . . . .	18
3.2.11	SRM booster: propellant choice . . . . .	19
3.2.12	SRM booster: flight performance . . . . .	20
3.2.13	SRM booster: nozzle dimensioning . . . . .	20
3.3	Weight . . . . .	21
3.3.1	Warhead design . . . . .	21
3.3.2	Ramjet mass evaluation . . . . .	22
3.3.3	Booster mass evaluation . . . . .	23
3.3.4	Center of mass . . . . .	24
3.4	Trajectory . . . . .	24
3.4.1	Flight motion modelling . . . . .	25
3.4.2	Guidance and control system . . . . .	26
3.5	Structural analysis . . . . .	26
3.5.1	External structure thickness . . . . .	26
3.5.2	Frequency analysis . . . . .	27
3.5.3	Compatibility with the helicopter . . . . .	27

3.6	Monte Carlo simulation . . . . .	27
3.6.1	Wind . . . . .	27
3.6.2	Missile Mass . . . . .	28
3.7	Final considerations on stability . . . . .	29
<b>4</b>	<b>Concluding remarks</b>	<b>30</b>
<b>A</b>	<b>House of Quality and Risk Matrix</b>	<b>33</b>
<b>B</b>	<b>Helicopter data</b>	<b>34</b>
<b>C</b>	<b>Isentropic flow and Shock Waves</b>	<b>35</b>
<b>D</b>	<b>Nozzle contraction ratio</b>	<b>37</b>
<b>E</b>	<b>Pylon preliminary design</b>	<b>38</b>
<b>F</b>	<b>Structural Analysis</b>	<b>40</b>
<b>G</b>	<b>Theoretical analysis on a possible control system</b>	<b>41</b>
<b>H</b>	<b>Meteograms</b>	<b>43</b>
<b>I</b>	<b>Stability</b>	<b>45</b>

# List of Figures

1.1	Render overview of the missile . . . . .	1
2.1	Design flow . . . . .	3
2.2	Project management triangles. . . . .	4
2.3	Technological risk matrix. . . . .	4
2.4	Management risk matrix. . . . .	4
2.5	Image of the <i>Kh-31A "Krypton"</i> missile. . . . .	5
3.1	Drag coefficients as function of the Mach number. . . . .	9
3.2	Tail drag coefficients as function of the Mach number. . . . .	10
3.3	Inlet without spillage. . . . .	14
3.4	Relationship between shock wave angle, deflection angle and Mach number. . . . .	14
3.5	Engine flow path design . . . . .	15
3.6	Integrated rocket ramjet configuration. . . . .	18
3.7	Typical solid propellants for missiles. . . . .	19
3.8	Different contributions to the center of mass. . . . .	24
3.9	Typical sea skimming trajectory . . . . .	25
3.10	Detail of the two manoeuvres . . . . .	25
3.11	Monte Carlo simulation with wind perturbation. 1000 trajectories outlined, between red markers are 68% trajectories with a standard deviation of 274.4073m, between blue markers are 97% trajectories with a standard deviation of 548.8146m. The target is at the centre. . . . .	28
3.12	Descending phase . . . . .	29
3.13	Cruise phase . . . . .	29
A.1	House of Quality of the project. . . . .	33
B.1	Launch platform is the helicopter SH-60 of the US navy. . . . .	34
D.1	Booster nozzle . . . . .	37
E.1	Render UH60-BlackHawk. . . . .	38
E.2	Pneumatic Bomb Ejection Rack . . . . .	39
E.3	Static bending moment calculated on ground. . . . .	39
F.1	Shear forces and bending moment with respect to the nosecone during boost phase.	40
F.2	First bending frequency for different values of thickness. . . . .	40
G.1	Block diagram of the control system . . . . .	42
H.1	Typical Europe Wind Chart . . . . .	43
H.2	Detailed wind direction in the Mediterranean target location . . . . .	44
H.3	Wind vectors from Jun to Dec 2020 . . . . .	44

I.1	Center of pressure position without flare.	45
-----	--	----

# List of Tables

2.1	Baseline parameters.	5
2.2	Additional baseline parameters.	5
2.3	Results of the sensitivity analysis.	6
3.1	Drag coefficients.	9
3.2	Characteristics of conventional ramjet fuels.	12
3.3	Fuel input data.	12
3.4	Upstream airflow conditions.	12
3.5	Shock Waves	15
3.6	Combustion initial guess	16
3.7	Combustion chamber parameters	17
3.8	Inlet integration	18
3.9	Specific impulse.	18
3.10	Thrust.	18
3.11	Engine efficiency	19
3.12	Results from CEA code.	19
3.13	Nozzle estimation	20
3.14	Nozzle dimensions	21
3.15	Manoeuvres data	25
4.1	Final result of preliminary design	30
B.1	Main SH-60 data.	34
C.1	Rayleigh combustion in cruise phase	35
C.2	Shock conditions at Mach 2.5-3	36
C.3	Shock conditions at Mach 3	36

# Nomenclature

$\langle \sigma \rangle$	Standard deviation	[ ° ]
$\alpha$	Angle of attack	[ ° ]
$\delta$	Deflection angle	[ ° ]
$\delta_{LE}$	deflection angle of the tail	[ ° ]
$\Delta v$	Speed variation	[ m/s ]
$\dot{m}$	Mass flow rate	[ kg/s ]
$\epsilon$	Nozzle expansion ratio	[ - ]
$\epsilon_s$	Booster structural ratio	[ - ]
$\eta$	Efficency	[ - ]
$\gamma$	Heat capacity ratio	[ - ]
$\lambda$	Lagrangian multiplier	[ - ]
$\rho$	Density	[ kg/m³]
$\sigma$	Stress	[ MPa ]
$\theta$	Shock wave angle	[ ° ]
$A$	Area	[ m² ]
$a_0$	Speed of sound	[ m/s ]
$c^*$	Characteristic velocity	[ m/s ]
$C_D$	Drag coefficient	[ - ]
$c_f$	Thrust coefficient	[ - ]
$C_L$	Lift coefficient	[ - ]
$c_N$	Normal force coefficient	[ - ]
$c_P$	Heat capacity at constant pressure	[ kJ/kgK ]
$C_{D0}$	Zero-lift drag coefficient	[ - ]
$D$	Drag	[ N ]
$d$	Diameter	[ m ]
$E$	Young modulus	[ GPa ]

$F$	Force	[ N ]
$f$	Frequency	[ Hz ]
$f/a$	Fuel-to-air ratio	[ - ]
$f_k$	Objective function	[ - ]
$F_{\Delta v}$	Force required for acceleration	[ N ]
$g$	Maximum loading factor	[ g ]
$g_0$	Gravity acceleration constant	[ m/s <sup>2</sup> ]
$h$	Altitude	[ m ]
$H_f$	Combustion heating	[ kJ/kg ]
$I_s$	Specific impulse	[ s ]
$L$	Lift	[ N ]
$l$	Length	[ m ]
$L/D$	Aerodynamic efficiency	[ - ]
$l/d$	Fineness ratio	[ - ]
$l_n/d$	Nose fineness ratio	[ - ]
$M$	Mach number	[ - ]
$M_0$	Initial mass	[ kg ]
$m_b$	Bending moment	[ Nm ]
$M_f$	Final mass	[ kg ]
$M_p$	Propellant mass	[ kg ]
$M_s$	Structural mass	[ kg ]
$MM$	Molar mass	[ g/mol ]
$N_{rot}$	Rotations per minute	[ rpm ]
$p_i$	Static pressure	[ Pa ]
$p_{Ti}$	Total pressure	[ Pa ]
$q$	Dynamic pressure	[ N/m <sup>2</sup> ]
$r$	Radius	[ m ]
$R0$	Gas constant	[ J/kgK ]
$SF$	Safety factor	[ - ]
$T$	Thrust	[ N ]
$t$	Thickness	[ m ]
$T_i$	Temperature	[ K ]

$T_{Ti}$	Total temperature	[ K ]
$v$	Speed	[ m/s ]
$W$	Weight	[ kg ]
$w_k$	Relative weight	[ - ]
$G(x)$	Scalarized function	[ - ]

# Chapter 1

## Introduction

The aim of this report is the description of a conceptual design study on an air-launched anti-ship missile, based on ramjet technology and compatible with the SH-60 helicopter.

The objective of the *Sea Harvester* project is to develop an integrated solid rocket ramjet, able to strike down targets up to a distance of 75 km from the launch platform. The latter is placed at 1 km of altitude, moving at 250 km/h. To achieve this goal, the missile is designed to detonate a 250 kg warhead, after an impact with the enemy ship at Mach 3.



**Figure 1.1:** Render overview of the missile

### 1.1 Mission scenario definition

The starting point is the definition of the high-level objectives of the project, defined with the customer. They will be a mix of programmatic requests and performance needs, which will drive the technology push of the project. The customer's main requests are:

- Launch platform: Seahawk SH-60b, at 1000 m of altitude and 250 km/h of speed;
- Warhead weight: 250 kg;
- Terminal velocity: Mach 3;
- Range: 75 km.
- Engine: SRM/Ramjet

Before the beginning of the technical development of the missile, some considerations about the project management are done, starting from the aforementioned requirements, in order to expedite the whole process.

## Chapter 2

# Project Management

Conceptual design and system engineering is an iterative process, requiring a number of design iterations to achieve a balance of emphasis from different inputs and outputs. In this missile project, the major tasks of technical design are:

- Mission and scenario definition;
- Weapon requirements and sensitivity analysis;
- Integration of the missile with the launch platform;
- Propulsion technology;
- Risk analysis;
- Conceptual design synthesis and development roadmap.

The customers' mission requirements demand to be a trade-off between available technology and specified strategic targets.

The high-level requirements, which were initially provided by the military customer, are an input for the system modelling, in order to provide a higher definition and allocation of the mission. This engineering model deals with a single launch platform, and a single missile with a specified target.

The physical integration of the missile with the launch platform provides constraints, such as the length and weight of the rocket and the carriage environment: temperature, gusts, vibrations, and loads.

The missile is reconfigured through an iterative process, in which its characteristics are progressively evaluated. Some of the most important parameters that should be considered are: the aerodynamic shape, propellant or fuel type and weight, flight trajectory, range and interception time, accuracy, reliability, and cost. For instance, a parameter would be the quantity of propellant, or fuel, that should be added to match the flight range requirement.

The project must follow the clear workflow necessary to expedite the design process. Based on the mission requirements, an initial baseline from existing missiles with similar propulsion is established. This is a starting point to achieve the design convergence, in order to satisfy the iterative process represented in Fig. 2.1. The main goal is to create a balanced system engineering for our missile, using an accurate benchmark based on real data, and to develop a coherent conceptual design assessing the flight performance requirements.

In the iterative evaluations performed by this method, the aerodynamic part is an investigation for different choices of geometry configuration. Then, the output of the aerodynamic computation is the starting point for the propulsion system design, beginning with the size of the subsystem itself. The most efficient propellant, or fuel, will be a priority to meet the range and time-to-target requirements.

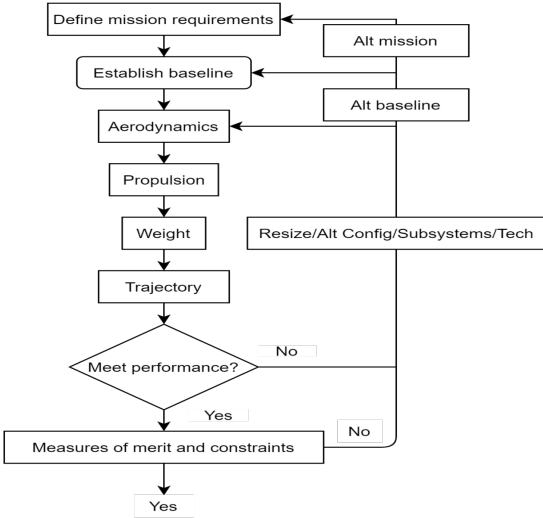


**Figure 2.1:** Design flow

Clearly, at this point, the weight estimation of the new missile, with respect to aerodynamics and propulsion, is mandatory to manufacture the rocket. As a final step, it is possible to evaluate the flight trajectory. Had the missile design not matched the flight performance requirement, alternative configuration, subsystems or technologies could be taken into account, and might be resized for the next iteration and evaluation.

In conclusion, the missile design activity is an opportunity to harmonize different inputs early in the development process.

## 2.1 House of Quality

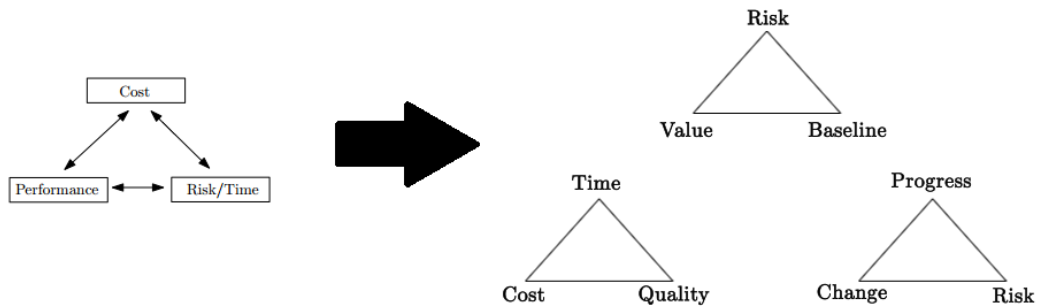
A useful tool to achieve a robust design is to construct a “House of Quality”. The definition of an optimal choice, usually, is not allowed because of the coeval presence of programmatic and performance requirements, thus having them to contradict one another. Therefore, the house of quality method comes in hand, to support the generation of technical specifications from the customer’s requirements. The team’s analysis of the first house of quality provides a preliminary look on strengths and weaknesses of the solution adopted.

Figure A.1, in Appendix A, shows the House of Quality related to this project. Firstly, after a discussion with the customer, it turned out that the compatibility with the helicopter is the most relevant requirement, having a maximum importance of 9, whereas the goal value of the mass of the warhead is not so strict. As we can see from the results of the House of Quality, obtained by taking into account the weight given to each customer requirement and the correlation relationship with the functional requirements, the key physical parameter is the total mass of the whole system, followed by the slenderness ratio  $l/d$ , both characterized by high relative weights. Overall, every mass contribution is significant to the final outcome, as well as the range. These results highlight the most critical parameters to focus on during the design phase, and they will be discussed later by means of the Pareto sensitivity analysis. Another consideration, obtained from the HoQ, is linked to the competitors: the system must be designed in order to compete with the market, focusing especially on the top level requirements such as the compatibility. Finally, looking at the top roof of the HoQ, it is clear that a trade-off analysis is needed: in fact there are both positive and negative correlations between the technical requirements direction of improvement, which means that the optimization of a certain parameter can be obtained only at expense of another one. For instance, the minimization of the propellant mass implies a reduction of the range.

## 2.2 Risk analysis

Considering the initial stage of the project, it is clear that risk, defined as the eventuality that the results of the project could differ from the customers' requirements regarding a specific given task, represent an inner threat for the project itself. At first, the variability and the lack of information concerning the project parameters, such as time and cost, are the first factors to pick in the risk management. Secondly, the dimensions and the complexity of the project, such as the presence of innovative technology, could be a source of hazards in the iterative design process of the missile.

Usually, there are three fundamental elements in project management: cost, performance, and time. In this case, costs are not mentioned by the customer to be an important goal to meet: the project is more concerned about developing a robust design with low risk, which also matches certain minimum performances. A deeper analysis shows that the project is a larger ensemble than just the traditional parameters, as shown in Fig. 2.2.



**Figure 2.2:** Project management triangles.

In order to evaluate the risk from a quantitative point of view, it is possible to express in a matrix the relationship between the success probability of one parameter, from a specific subsystem, and the impact magnitude of the very same parameter, from a numerical point of view. This is tabulated for each priority parameter in Fig. 2.3 and 2.4.

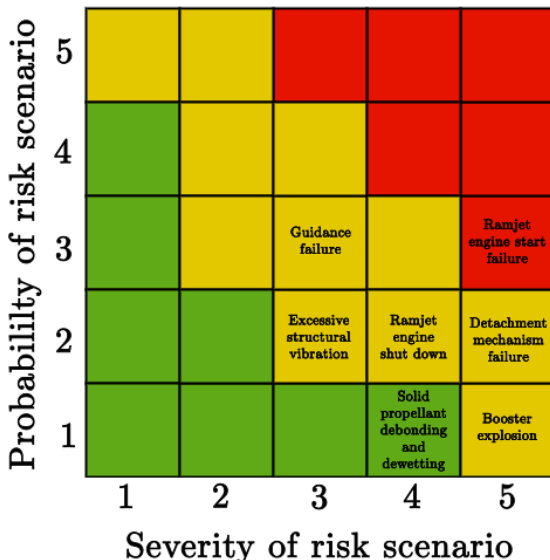


**Figure 2.3:** Technological risk matrix.

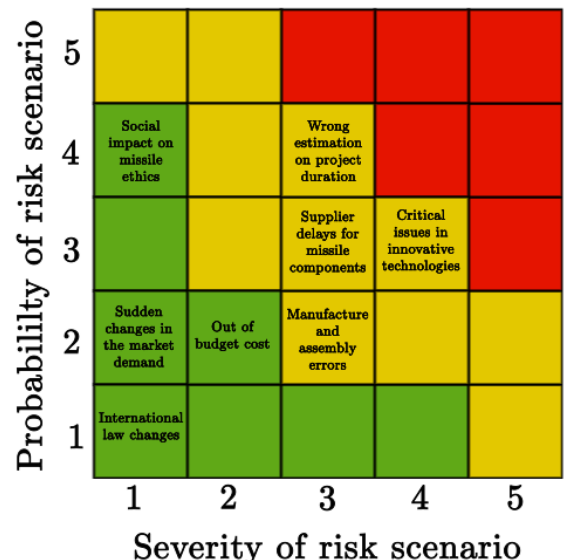


**Figure 2.4:** Management risk matrix.

## 2.3 Baseline Design

As previously discussed, starting with a good baseline enhances the accuracy and speed of the missile design and system engineering process. Since a baseline missile is one that includes real data, it allows corrections to simple design methods, such that they can be used with reasonable accuracy. Clearly, the existing documentation for a specified missile provides traceability between cause and effect, as the conceptual design and system engineering process is conducted. Hence, the start-up time for conceptual design is greatly reduced.

The initial input values for the missile conceptual design are the baseline missile data. However, a single baseline missile may not cover the overall range of possible solutions. In this case, the baseline missile flight performance parameters should be comparable to that of the conceptual design missile, considering that the reference features can usually be extrapolated about  $\pm 50\%$  with reasonable accuracy. For instance, considering a ramjet propulsion system, thrust is a function of Mach number, altitude, and fuel-to-air ratio. Moreover, maximum flight range is a function of the launch Mach number, launch altitude, cruise Mach number, and cruise altitude. All these parameters, with related dependencies, are developed in the house of quality, as shown in Fig. A.1, through a consensus with the customer on the most important requirements and their relative weighting.

One possible missile, which can be considered as a baseline, is the Russian *Kh-31A* "Krypton", an anti-ship configuration for the missile *Kh-31*. Some of its parameters are listed in Table 2.1 and 2.2.

**Table 2.1:** Baseline parameters.

Engine	Mass [kg]	Length [m]	Diameter [mm]	Warhead [kg]	Range [km]	Max speed [Mach]
Boost: solid fuel rocket	600	4.7	360	90	25-110	3.5
Sustain: liquid ramjet						

**Table 2.2:** Additional baseline parameters.

Guidance System	Speed at launch [km/h]	Altitude at launch [km]	Wingspan [mm]
inertial guidance with active radar homing	600-1100	0.1-10	778



**Figure 2.5:** Image of the *Kh-31A* "Krypton" missile.

## 2.4 Sensitivity analysis

As already stated, the design process is an iterative process dealing with large-scale problems and different goals to be achieved. In the vast majority of the cases, not every aspect of the project can be optimized, especially when these aspects are opposing each other. These types of problems are the subject of multicriteria optimization, which concerns mathematical optimization problems, involving more than one objective function to be optimized simultaneously.

When multiple conflicting objectives should be achieved, in the presence of trade-off between two or more concurrent cost functions, it can be difficult to take an optimal decision, because the contemporary minimization of all objective functions is unfeasible. In this case, a Pareto solution represents a sub-optimal solution, since, from that point, none of the objective functions can be improved without degrading some of the others.

The design of a rocket is a perfect example of multicriteria optimization, with a lot of different cost functions which could be taken into account. The starting point will be the scalarization (a priori method): in this way, the problem is reduced to a scalar problem so that the solution is Pareto optimal. In this project, a *linear scalarization* is used:

$$\text{Min} \sum_k w_k f_k(x) \quad (2.1)$$

where  $w_k$  are the relative weights and  $f_k$  are the objective functions. For this analysis, the objective functions considered are the range and the mass ratio, considering the importance they have in the House of Quality, from which their relative weights are defined. Therefore, the scalarized function is:

$$G(x) = w_1 \frac{M_0}{M_f} + w_2 I_s v \frac{C_L}{C_D} \log\left(\frac{M_0}{M_f}\right) \quad (2.2)$$

Then, a sensitivity analysis is conducted with respect to  $G(x)$ : the aim is to reduce the number of design variables and to understand which contribute more to the success of the project. The analysis is conducted through direct differentiation, evaluating the partial derivatives in the design point. Since there are some still unknown variables, like  $C_L$  or  $M_P$ , all the variables are evaluated through the design point of the baseline missile (to obtain the value of  $M_P$ , a structural ratio of  $\frac{M_S}{M_0} = 0.22$  is considered). The results of the analysis are shown in Table 2.3.

**Table 2.3:** Results of the sensitivity analysis.

	$I_s$	$v$	$C_D$	$C_L$	$M_0$	$M_P$	Total
	10	10	-10	10	-35.12	35.12	110.24
Relative weight	0.091	0.091	-0.091	0.091	-0.318	0.318	1

From these results, the four variables  $M_P$ ,  $M_0$ ,  $C_D$ , and  $C_L$  sum up for the 81.6% of the total weight. Considering the 80/20 rule, these variables will be the most important in the design process, while  $I_s$  and  $v$  will be less significant, especially because  $v$  already has an assigned value and  $I_s$  depends on the type of propulsion chosen.

# Chapter 3

## Conceptual design

### 3.1 Aerodynamics

Once mission requirements are defined and a baseline missile is established, the following step is to perform the aerodynamic configuration synthesis, which requires a consideration of alternative layouts, aerodynamic technology, and the process of resizing the missile. The outputs will be the missile body dimensions, such as its diameter, length and nose geometry. After more complex aerodynamic considerations, which are outside the tasks of this project, it is possible to choose the most suitable control surfaces for the missile. In appendix G, a control system has been proposed. The final output of the aerodynamic configuration activity will be the input to the propulsion system design.

#### 3.1.1 Predicting missile aerodynamics

The first aerodynamic input is the missile diameter, which must be seen as a trade-off between benefits and drawbacks of different dimensions. The advantages of a small diameter missile include lower drag and smaller cross section dimensions for the compatibility with the launch platform, in lateral constraint terms. On the other hand a large diameter missile is fit to carry a greater payload, such as better guidance system; this provides the missile the possibility to operate on an increased signal range, with higher resolution, and a better tracking in the case of a ‘seeker’. The figure of merit for such specifications, with respect to the selected baseline, is the missile body slenderness ratio ( $l/d$ , length-to-diameter ratio). Typically, the ratio is higher than 5-8 for stabilization concerns, and lower than 20-25 due to structural issues. In order to provide lower drag in supersonic flight and to pack the propellant volume for such flight conditions, the final choice is oriented to a relatively greater length and a smaller diameter. In this case, from a baseline review, the slenderness ratio is selected to be 14.

#### 3.1.2 Nose fineness and geometry compromise

Another consideration that should be done for the aerodynamic approximation is the missile nose fineness and geometry. A high-fineness nose, such as  $l_N/d = 5$ , is ideal for low supersonic drag, and it corresponds to a low radar cross section. Vice versa, a low-fineness nose, such as  $l_N/d = 0.5$  corresponding to a hemispherical nose, is ideal for an electromagnetic seeker, and it leaves more space for propellant storage in length-limited missiles, but it clearly carries an increased aerodynamic drag. Considerations about a guidance system will be done later in the report.

In conceptual design analysis, it is important to consider that supersonic drag is usually more sensitive to nose fineness than to nose geometry. As a first approximation, a tangent ogive nose, with a circular arched surface, will be considered. In order to respect the mission requirements,

and as suggested by the selected initial baseline, it is possible to define a high-fineness nose, ideal for low supersonic drag, equal to 4.

A tangent ogive nose has relatively low supersonic drag, and a relatively low cross section of the radar. The curved surface of a tangent ogive results in a very likely electromagnetic and optical distortion, with the effect of having errors in tracking the target.

### 3.1.3 Total drag prediction

Regarding the solution of the aerodynamic problem, it is necessary to compute the aerodynamic force acting on the missile. Considering the aerodynamic drag, it is possible to deal with the problem by estimating the total zero-lift drag coefficient of a body as the sum of skin friction drag, base drag, and wave drag, under the obvious assumption of a supersonic flow.

$$(C_{D0})_{Body} = (C_{D0})_{Body,Friction} + (C_{D0})_{Base} + (C_{D0})_{Body,Wave} + (C_{D0})_{Tail} \quad (3.1)$$

According to this theoretical prediction, an initial definition of the nose geometry is fundamental. A sharp corner nose is not feasible with nowadays technologies. In addition, a small amount of nose tip bluntness is desirable to decrease local stress concentration and tip heating. Clearly, for a guidance system control constraint, as mentioned above, this configuration is not achievable. The difficulty in modelling a blunt nose can be simplified by relating blunted nose to cone and hemispherical ones (Eq. (3.2)). In any case, in the very preliminary aerodynamic prediction phase, a tangent ogive nose has been considered for aerodynamic convenience. Now, it is assumed that a 10 % diameter of the missile is used for a new approximation of the nose geometry.

$$(C_{D0})_{Body,WaveBlunt} = (C_{D0})_{Body,WaveSharp} \frac{A_{ref} - A_{nose}}{A_{ref}} + (C_{D0})_{Body,WaveHemi} \frac{A_{nose}}{A_{ref}} \quad (3.2)$$

$$(C_{D0})_{Body,WaveSharp} = \left( 1.586 \frac{1.834}{M^2} \right) \left[ \arctan \left( \frac{0.5}{l_N/d} \right) \right]^{1.69} \quad (3.3)$$

$$(C_{D0})_{Body,WaveHemi} = 0.665 \left( 1.586 \frac{1.834}{M^2} \right) \quad (3.4)$$

During powered flight, the base drag is reduced by the factor  $(1 - A_e/A_{ref})$  (Eq. (3.5) and 3.6). If the nozzle exit area is nearly as large as the missile base area, the base drag may be negligible during powered flight. Base drag can be a major contributor to the total drag during an eventual costing flight phase, because of the low pressure in the base, but in this case, according to the mission design, the missile will always be powered. Therefore, a low contribution of base drag is expected from computational analysis, which has been performed in *Matlab*.

$$(C_{D0})_{Base,Powered} = \left( 1 - \frac{A_e}{A_{ref}} \right) \frac{0.25}{M}, \quad \text{supersonic} \quad (3.5)$$

$$(C_{D0})_{Base,Powered} = \left( 1 - \frac{A_e}{A_{ref}} \right) (0.12 + 0.13M^2), \quad \text{subsonic} \quad (3.6)$$

Finally, skin friction drag is a major contributor to subsonic drag, and it is primarily driven by the body fineness ratio, as reported in Eq. (3.7). Besides, a dependence by the Mach number, the dynamic pressure, and the body length is verified, but in a weak form.

$$(C_{D0})_{Body,Friction} = 0.053 \left( \frac{l}{d} \right) \left( \frac{M}{ql} \right)^{0.2} \quad (3.7)$$

Some assumptions need to be done for the body friction drag equation: the body wetted area of a non-circular body can be approximated by the wetted area of an equivalent circular cross section cylinder. Furthermore, the variation in the free stream speed of sound and viscosity with

respect to altitude must be relatively small, and the flow over the body must have a turbulent boundary layer. In addition, this equation assumes that there is no boattail. Nevertheless, as the motors will always be powered, a configuration without boattail is not a disadvantage for the forecast mission.

A slightly positive angle of attack during the cruise phase could be a good choice due to the fact that, with such attitude, the body generates a non-negligible amount of lift, therefore a smaller wing area is needed. Thus, the cross section is reduced, giving it the ability to be less visible by radar interceptions.

Fig. 3.1 shows the generic drag coefficient dependence for a body angle of attack  $\alpha$  of  $0.5^\circ$  (a very low one, not compatible with the descent phase of the boost), but the overall trend is thoroughly useful for the conceptual design of the missile, in a first aerodynamic drag estimation. For simplicity, the ramjet cruise phase is analysed at Mach 3, with a tail angle of attack<sup>1</sup>  $\alpha' = \alpha + \delta_{LE} = 0.5^\circ - 0.2385^\circ = 0.2615^\circ$ .

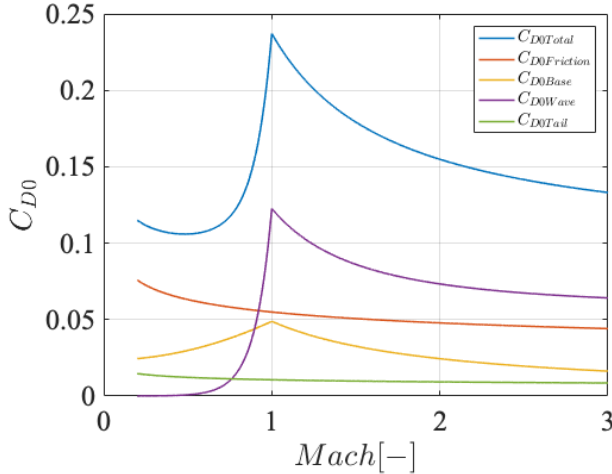


**Figure 3.1:** Drag coefficients as function of the Mach number.

Considering an initial acceleration phase for the ramjet between Mach 2.5 and Mach 3, it is possible to notice that the contribution of drag, depending on the above mentioned components, is more or less the same of the cruise phase one.

In Fig. 3.1, it can be clearly noticed that at transonic and supersonic speed, even with a fineness nose ratio of 4, the wave drag on the nose is a major contributor on the total drag.

The contribution of tail drag, with respect to the global aerodynamic drag of the missile, is not a determining issue for the flight behaviour of the missile. It is possible to notice, as shown in Fig. 3.1, where the  $C_{D0}$  related to tail is much less than other drag contributions affecting the body.

Note that, during the cruise stage, not only have the vertical forces to be balanced, but the moments as well. Fig. 3.1 assures a nearly perfect equilibrium of moments at Mach 3, and a small but controllable unbalance moment at Mach 2.5. The angle which guarantees the balance of the aerodynamic moments is a bit different with respect to the one chosen for the dynamic equilibrium, which is  $\delta_{LE} = 0.9160^\circ$ . During this simulation, the deflection of the tail surfaces  $\delta_{LE}$  is kept constant. Instead, the Mach speed of 3 would need another angle of deflection of the tail to reach the equilibrium of moments. However, this graph also shows the different drag behaviours at which the missile will be subjected during his trajectory. Especially in the transonic zone, where a peak of the drag is expected.

**Table 3.1:** Drag coefficients.

	$M = 2.5$	$M = 3$
$(C_{D0})_{Total}$	0.1416	0.1331
$(C_{D0})_{Body,Friction}$	0.0458	0.0441
$(C_{D0})_{Base}$	0.0196	0.0163
$(C_{D0})_{Body,Wave}$	0.0674	0.0642
$(C_{D0})_{Tail}$	0.0089	0.0085

<sup>1</sup> $\delta_{LE}$ , deflection of the tail.

### 3.1.4 Stabilizers: flare, wings and tails

It is chosen to give the missile a stable configuration. To ensure it, a tail has been added to the missile. This will shift the global centre of pressure backwards until it is behind the centre of gravity.

From the house of quality, the launch platform compatibility is to be considered the key parameter in preliminary aerodynamic choices. For this reason, wings are not taken into account. Clearly, a small wing has range advantages in low supersonic flight, and in moderate dynamic pressure.

A conventional trapezoidal tail, with an aft swept leading edge, is considered in the design preliminary analysis. This tail surface is often selected for missiles because it has higher control effectiveness. The planar surface geometry is fundamental for stability and control, as well as, in a minor form, for aeroelasticity stability. No serious weaknesses on other attributes are theoretically forecast for this configuration. A 45° degrees rotated-cruciform tail configuration is integrated for the missile.

An aerodynamic drag coefficient analysis has been performed for the tail-only, considering a preliminary angle of attack  $\alpha'$ . The coefficient is computed as a sum of wave and friction losses.

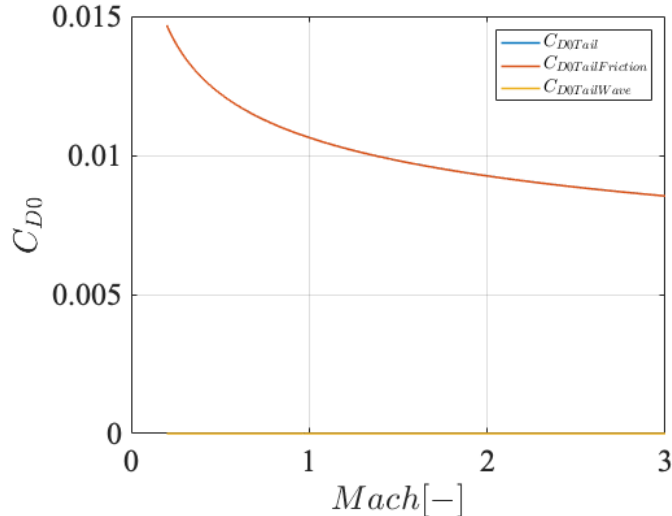


**Figure 3.2:** Tail drag coefficients as function of the Mach number.

In Fig. 3.2, it can be seen that, due to the very low deflection angle  $\delta_{LE}$  of the tail during the cruise condition, the wave drag is nearly equal to 0. Therefore, it can be said that the only contribution for the tail drag is friction; this is the reason why the blue line is overlapped with the orange one.

Subsequently in the conceptual design, it will be possible to evaluate the position of the centre of gravity. Thus, adjusting the dimensions of the stabilizer components and eventually adding a flare in case of problems, it is possible to obtain a stable missile.

## 3.2 Propulsion

Regarding the propulsion system, the design activity follows the prior sequences of defining mission requirements, establishing a baseline missile, and estimating the aerodynamic evaluation. In this process, a quick consideration to exploit alternative propulsion systems, alternative propulsion subsystems, and alternative technologies is needed. Finally, the propulsion system is sized. The output of this activity includes thrust, specific impulse, and propellant/fuel weight. Clearly, any propulsion definition is done starting with an approximate evaluation of the

dimensions of the combustor, the nozzle, and a reference fuel-to-air ratio. This is necessary to estimate the weight of the propellant, which has to meet the range requirement.

### 3.2.1 Propulsion considerations in the missile design

At first, a ramjet propulsion alternative with liquid fuel is considered, beside an integral rocket-ramjet configuration, with rocket booster occupying the same volume as the ramjet engine combustor. In ramjet propulsion, air enters the inlet at supersonic speed and is decelerated to low subsonic speed at the combustor entrance. Downstream of the combustor, there is a convergent-divergent nozzle, which accelerates the airflow back to supersonic speed. Regarding the maximum specific impulse, for a liquid hydrocarbon fuel ramjet, the value could be above 1400s. Since a ramjet engine is inefficient at low supersonic Mach numbers, a rocket booster is required to speed up the missile to the ramjet initial acceleration phase at about Mach 2.5.

The booster should accelerate the missile from the initial velocity of the launch platform site, which is  $250 \text{ km/h}$ , to Mach 2.5. In this case, the ramjet cruise at Mach 3 is preceded by an acceleration phase from Mach 2.5 to Mach 3. This is an important choice in order to save solid propellant and exploit the maximum potential of the ramjet engine. In this case, a limitation in the boost phase acceleration evinces in a smaller combustion chamber which is an advantage for both boost and ramjet phase. From a solid propellant viewpoint, the choice to limit the initial acceleration to Mach 2.5 permits an overall optimization on the length and weight of the entire missile; at the same time, a smaller combustion chamber is more convenient for the ramjet architecture, which would not need such a long combustor were the boost acceleration phase until Mach 3.

In the propulsion system choice, it would have been possible to consider a ducted rocket, which has a higher acceleration than a traditional ramjet and a greater range than a rocket. At first glance, the missile compatibility with the launch platform should be considered a priority, as indicated in the project management section. In fact, from the initial house of quality, realised alongside the customer, the compatibility is the most important parameter to be considered in order to match the mission requirements. A ducted rocket might not meet the length and diameter constraints imposed by the mission scenario.

In the case of an ideal ramjet, the thermodynamic cycle consists of an isentropic compression of the flow by the inlet, constant combustion pressure in the combustor, and isentropic expansion through a convergent-divergent nozzle to the free stream static pressure. The liquid fuel is injected in the header of the combustor.

The booster is ignited by a pyrotechnic system, while the ramjet uses a spark ignition system [3], which can be used multiple times if the engine needs to be re-ignited during the cruise, in case the internal sensors detect an unexpected shutdown.

### 3.2.2 Ramjet sustain: fuel choice

Conventional ramjet fuels are kerosene-type, with a complex mixture of different hydrocarbons which are combined with the oxygen from the inlet air. In the conceptual design of fuel propulsion scheme, JP-10, a hydrocarbon liquid fuel, has been considered especially for its relatively high heating value, and relatively high density, if the latter is compared to other JP fuels. Other advantages are low freezing temperature, safety, and availability. Another solution could be the choice of a different fuel, RJ-5 for instance, which could allow a greater performance. In particular, a higher density of this fuel could represent a significant advantage in the global mass for a missile, but a low freezing point and higher costs are parameters which led to the choice of not using it.

The ramjet path is at sea level conditions. After the aforementioned acceleration phase, the Mach number of the missile is constant, during the cruise stage, and equal to 3.

**Table 3.2:** Characteristics of conventional ramjet fuels.

Type	Fuel	Density [kg/m <sup>3</sup> ]	Volumetric performance [kJ/m <sup>3</sup> ]	Observability
Hydrocarbon	Ramjet (JP-4, JP-5, JP-7,JP-8, JP-10)	~ 858.07	~ 3.6 10 <sup>7</sup>	low

**Table 3.3:** Fuel input data.

Fuel-Air ratio	Combustion heating	Density	C <sub>p</sub>
0.04	43496.2 kJ/mol	940 kg/m <sup>3</sup>	1.28 kJ/kgK

The total pressure is obtained through the isentropic relation for a polytropic ideal gas:

$$\frac{P_{0T}}{P_0} = \left(1 + \frac{\gamma_0 - 1}{2} M_0^2\right)^{\frac{\gamma_0}{\gamma_0 - 1}} \quad (3.8)$$

As a first approximation, a slope angle in the boost phase is supposed to be around 40°, and a payload mass of about 250 kg is considered for this moment only. An area ratio equal to 10 is estimated to be an optimal compromise from baseline analysis.

### 3.2.3 Ramjet flight optimization L = W

Given the missile diameter, length and angle of attack, together with the nozzle diameter, it is possible to develop a *Matlab* optimization cycle. All the aerodynamic parameters are computed for the sustain phase in an iterative way, from the angle of attack of the tail wings  $\alpha'$ . Starting from a given  $\alpha'$ , the iteration of the cycle manages to determine, for the ramjet trajectory, an aerodynamic flight condition in which the weight of the missile is equal to the lift. The weight is the last parameter which will be determined in the conceptual design of the missile. This means that all the following computations, for the aerodynamic and propulsion subsystems, are performed considering an external iterative process, which will give a final value for the weight of the missile. This value is a partial output because it will be reinserted in the cycle until the desired flight condition will be achieved.

### 3.2.4 Ramjet sustain: supersonic/subsonic inlet integration

The inlet design considerations have a relatively large effect on the aerodynamic configuration conceptual design. The main goal for an aerodynamic optimization is to have inlets which capture 100% of the oncoming supersonic flow, with no spillage. In order to achieve such optimization, a mixed compression inlet is designed. This presents external oblique shocks, followed by internal oblique shocks. Mostly, this configuration is selected for supersonic missiles, because it is often

**Table 3.4:** Upstream airflow conditions.

Temperature [K]	Density [kg/m <sup>3</sup> ]	Pressure [Pa]	Heat ratio	Gas constant [J/kgK]	C <sub>p</sub> [kJ/kgK]	Total pressure [Pa]
288.15	1.125	101325	1.4	287	1.0045	3721900

a good compromise of relatively low deflection drag, relatively low-pressure oscillations, and relatively low inlet start Mach number.

Inlets spillage, which could be a serious threat, occurs at a lower Mach number. Here external shock waves occur with a high angle, passing over the inlet, so less of the free stream air is captured and spillage happens. This results in lower thrust and tends to increase drag. A deeper analysis on the spillage could be done in a further design phase in order to optimize the inlet for all the stages of the flight. Regarding the design of the inlet architecture, one priority is to have a higher upstream free flow Mach number condition, with shocks converging on the inlet tip, providing a higher thrust.

From an aerothermodynamic point of view, analyzing a normal or oblique shock wave inside the inlet becomes too complex. To avoid a supersonic inlet, which could not be considered as an ideal one, a final normal shock wave, at the inlet entry, is computed with respect to the requirement of non-spillage condition. In this case, the inlet works in subsonic conditions and a simplified internal configuration could be assessed.

It has been previously mentioned that, in order to optimize the weight and dimensions of the missile, the iterative procedure leads to the choice of splitting the total acceleration between the booster and the initial part of the ramjet flight. This means that the optimization of the aerodynamic relations, about an ideal subsonic inlet, must be done at Mach 2.5, even if most of the flight will be at Mach 3, in order to make the starting of the air inlet possible. For a conceptual design, in this condition only, an ideal no spillage configuration should be guaranteed. The aerodynamic efficiency is at its maximum at the activation of the inlet, since a subsonic Mach number is entering the inlet after the final normal shock wave, and the risk of a ramjet malfunction is greatly reduced. This initial constraint imposes a non-optimal compression in the inlet after the initial acceleration phase, since the geometry of the missile nose permits a combination of shock waves and subsequent no spillage condition for a specified Mach value only. It is clear that, during the cruise phase at Mach 3, the ramjet will not work in an optimized condition. This could be noticed in the propulsive efficiency, which is lower than the maximum possible for this type of engine. Although this choice leads to a loss in thrust performance, it is still convenient because of a great gain in terms of weight, which is an important parameter for the compatibility with the launch platform, and production cost.

In conceptual design terms, it is more appropriate to consider, at this point, an external compression with no spillage. The advantage is to obtain a relatively low-pressure oscillation inside the inlet, beyond the inlet start Mach number, as aforementioned. Approximations in drag losses, from the forebody inclination angle, are considered in the wave nose drag, discussed in the aerodynamic part of the conceptual design iterative process. A thrust loss for off-design flight conditions is not negligible anymore, since the operating range of the ramjet is at constant altitude but not at a constant free stream Mach number, due to the acceleration initial phase implemented in the missile design.

To achieve a shock-on-lip condition, it is reported below a relationship of the oblique shock wave  $\theta$  to the flow deflection angle ( $\alpha + \delta$ ) and Mach number M.

$$\tan(\alpha + \delta) = \frac{2 \cot(\theta_{2D})(M^2 \sin^2(\theta_{2D}) - 1)}{[2 + M^2(\gamma + 1 - 2 \sin^2(\theta_{2D}))]} \quad (3.9)$$

This aerothermodynamic equation assumes a two-dimensional flow of a perfect gas. The shock wave angle increases with body deflection angle and decreases with the Mach number. As a result, the inlet height, to avoid air spillage, must be larger for a missile with a low fineness nose at a low supersonic Mach number. Clearly, the maximum allowable flow deflection increases with Mach number. In the acceleration phase of the ramjet, starting at Mach 2.5, it is important to consider the maximum allowable flow deflection angle to have an attached two-dimensional oblique shock. In this case, for a 2.5 Mach number, an angle of attack of 0.5°, and  $\gamma=1.4$ ,  $(\alpha + \delta)_{MAX} = 29.8^\circ$ . Whereas at Mach 3, that condition is achieved for  $(\alpha + \delta)_{MAX} = 34^\circ$ .

◆ **External compression inlet w/o spillage**

- Inlet swallows 100% of the free stream flow
- Shock waves converge at inlet cowl lip (inlet captures maximum free stream flow)

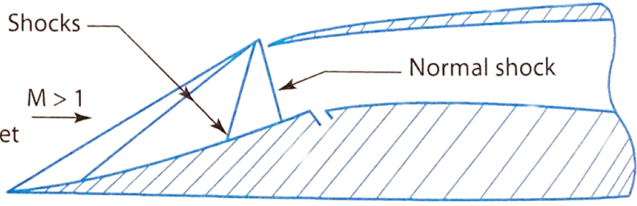


**Figure 3.3:** Inlet without spillage.

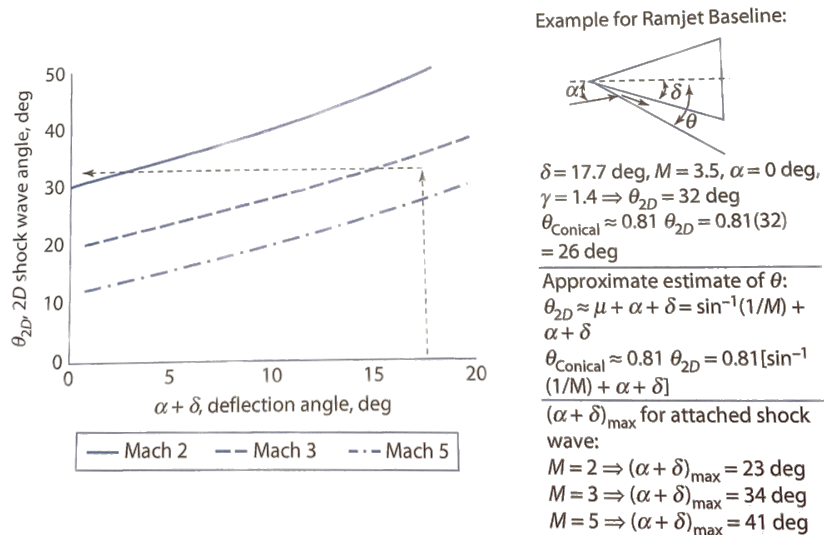


**Figure 3.4:** Relationship between shock wave angle, deflection angle and Mach number.

A first estimation of the two-dimensional shock wave angle, necessary for conceptual design, is to assume that the shock wave angle  $\theta_{2D}$  is the sum of the Mach angle plus the flow deflection angle  $(\alpha + \delta)$ . From an aerothermodynamic relation, the approximate equation is  $\theta_{2D} \approx \arcsin(\frac{1}{M} + \alpha + \delta)$ . This last equation becomes inaccurate for body deflection angles  $\delta > 20^\circ$ . From the geometry of the missile, an initial deflection angle of  $\delta = 17.7^\circ$  is taken into account for the 2D analysis of the aerothermodynamic problem, and an angle of attack of  $0.5^\circ$  has been added for the correct computation of the oblique/normal shock waves. A combination of 3 oblique shocks and a final normal shock in front of the inlet, which is an optimal configuration for an external compression, is considered for the aerodynamic point of view.

The three oblique shock waves, shown in Table 3.5, are followed by a final normal shock wave which guarantees subsonic conditions in the inlet. This implies that, for the conceptual design of aerodynamic and propulsion subsystems, an ideal only divergent inlet is considered for the missile. In appendix C, static pressures and temperatures, alongside the corresponding Mach numbers, are shown as an input for the combustion chamber computations. In Table C.2, the reference for the flow condition is at Mach 2.5, which is the starting point for the inlet at

**Table 3.5:** Shock Waves

Shock wave	$\alpha + \delta$ total deflection angle	$\theta(M = 2.5 - 3)$ shock wave angle	$\theta (M=3)$ shock wave angle
Oblique 1	18.2°	37.84°	35.69°
Oblique 2	13.3°	45.18°	41.28°
Oblique 3	4.8°	50.59°	43.99°

the beginning of the acceleration phase of the ramjet. For the sake of simplicity, a mean value of the Mach number is considered for the acceleration phase. In further design processes, the acceleration stage could be integrated point by point. While, in Table C.3, the same parameters are referring to the ramjet cruise phase at Mach 3.

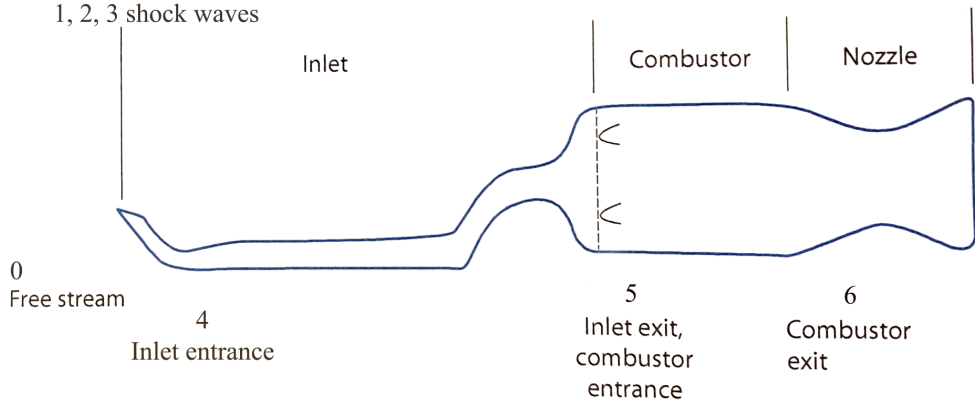


**Figure 3.5:** Engine flow path design

In a deeper analysis for conceptual design in 3 dimensions, it is possible to say that for a conical flow, around a conical nose, the shock wave angle is  $\theta_{conical} \approx 0.81 \theta_{2D}$ . As a reference, in Fig. 3.4, it is reported the relationship between the shock wave angle, the deflection angle, and the Mach number. This should be considered as an additional reference baseline for the aerodynamic and propulsion conceptual design.

As a final consideration, the inlet must be closed by some port covers during the boost phase. The most commonly used port covers are segmented collapsible, formed by structural beams held together by a rubber-like retention boot [4]. This type of cover falls to small pieces which are ejected through the nozzle at the end of the boosting phase.

### 3.2.5 Ramjet sustain: combustion temperature

For a ramjet combustion flow, the exit temperature  $T_6$  is a function of the free stream Mach number  $M_0$  and fuel-to-air ratio  $f/a$ . Hence, Eq. (3.10) used in the computational procedure is reported for a better explanation.

$$T_6 \approx T_0 \left[ 1 + \frac{\gamma_0 - 1}{2} M_0^2 \right] + \left( \frac{H_f}{c_p} \right) \left( \frac{f}{a} \right) \quad (3.10)$$

In the equation,  $T_0$  is the free stream static temperature,  $\gamma_0$  is the free stream specific heat

ratio,  $H_f$  is the fuel heating ratio, and  $c_p$  is the air specific heat ratio at constant pressure in the combustor. Low subsonic combustion and no heat transfer through the inlet are considered. As a last note, the fuel-to-air ratio is less than stoichiometric.

The resulting  $T_6$ , from Eq. (3.10), has just a theoretical meaning and it will be used as the initial guess for an optimization cycle in which the combustion temperature will be evaluated in order to match the flight conditions. It is now reported the guess value for the cruise phase of the ramjet at Mach 3.

**Table 3.6:** Combustion initial guess

Free stream Mach number	Static combustion temperature [K]	fuel-to-air ratio
3	$T_6=2362.4$	0.04

### 3.2.6 Ramjet cruise flight optimization $\mathbf{T} = \mathbf{D}$

Given the global  $C_{Dsustain}$  and the free stream flow condition ( $\rho_0$ ,  $M_0$ ,  $T_0$ ), and knowing the missile diameter, it is possible to compute the aerodynamic drag applied on the body during the cruise phase at Mach 3. At this point, a new *Matlab* sub-cycle is formulated in order to evaluate the correct temperature in the combustion chamber. In fact, the previously computed temperature in the combustor,  $T_6$ , must be verified such that it corresponds to the flight condition in which thrust is equal to drag.

Imposing the equality between the thrust and the drag coming outside the iterative process, it is now possible to compute the Mach number at the exit of the combustion chamber considering an isentropic flow between the end of the combustor and the nozzle throat area. The ratio between the exit area of the combustion chamber and the throat area of the nozzle is imposed equal to 10.

The nozzle dimensioning and the evaluation of the aerothermodynamic parameters related to the isentropic flow are computed later in the cycle, when the boost phase is better described.

### 3.2.7 Ramjet acceleration flight optimization $\mathbf{T} = \mathbf{D} + \mathbf{F}_{\Delta v}$

The same procedure must be followed for the acceleration phase of the ramjet, from Mach 2.5 to 3. The considerations related to the optimization cycle apply in the same way for the cruise phase at constant Mach number. The only non-negligible difference is that, in the equality between thrust and drag, the  $\Delta v$  necessary for the acceleration must be taken into account, in order to achieve the final Mach target of the cruise phase. This means that, on the right side of the previous equality, a net force contribution must be added.

### 3.2.8 Aerothermodynamic relations for the combustor

Isentropic flow relations: appendix C.

The Mach number at the end of the combustion chamber is obtained numerically, integrating the isentropic relation Eq. (C.3) starting from the contraction ratio. At this point, it is possible to determine the velocity of the flow and the total temperature. The computation is working under the assumption of the ideal polytropic gas law. Subsequently the speed of the gas flow is only a function of the Mach number and the speed of sound after the combustion. At the same time, the total temperature at the end of the combustor is computed as a function of the Mach number, already mentioned above, and of the static temperature in the combustion chamber. This temperature has been computed in the previous paragraph in Eq. (3.10), and it is now the main variable of the sub-cycle until convergence is achieved. This means that the static

temperature in the combustor, determined only by an enthalpic relation, must be equal to the final temperature at the end of the cycle, which considers the equality between thrust and drag, and of the net force related to the necessary  $\Delta v$  for the acceleration phase.

Given the exit condition of the combustor, it is possible to determine the initial condition before combustion starts. Under the assumption of heat addition at a constant combustor cross sectional area and negligible friction, it is possible to consider a Rayleigh flow in the combustion chamber. Considering the total temperature at the beginning of the chamber, computed accordingly with an isentropic flow in the inlet, and the total temperature at the end of the combustor given by the previous isentropic relation, it is possible to correlate the entering Mach number as a function of the final Mach number only.

Rayleigh flow relations under the assumption of  $\gamma M_5^2 \ll 1$ :

$$\frac{p_{6t}}{p_{5t}} \approx \frac{\left(1 + \left(\frac{\gamma-1}{2}\right) M_6^2\right)^{\frac{\gamma}{\gamma-1}}}{1 + \gamma M_6^2}, \quad \frac{T_{6t}}{T_{5t}} \approx \left(\frac{M_6}{M_5}\right)^2 \left(1 + \frac{\left(\frac{\gamma-1}{2}\right) M_6^2}{1 + \gamma M_6^2}\right) \quad (3.11)$$

The two phases of the ramjet, acceleration and cruise, are evaluated separately for the combustion chamber. In particular, the fuel-to-air ratio is iteratively performed starting from the initial guess of  $f/a=0.04$  in both optimization cycles. For the acceleration stage, a  $f/a=0.0358$  is considered as final result. While, for the cruise phase, a quite lower  $f/a$  is expected, in fact  $f/a=0.0165$  is obtained.

**Table 3.7:** Combustion chamber parameters

	f/a	Exit static temperature [K]	Exit static pressure [Pa]	Exit Mach number
Acceleration Phase	0.0358	2121.6	$54.37 \cdot 10^5$	0.0589
Cruise phase	0.0165	1450.2	$76.57 \cdot 10^5$	0.0589

In the same way, evaluating the total pressure at the entry of the combustion chamber as a result of an isentropic flow inside the inlet, and given now the corresponding Mach number, it is possible to estimate the local static pressure using the already known isentropic aerothermodynamic relations. In conclusion, the local velocity of the flow before the combustion is now calculated as a function of the Mach number and the static temperature.

### 3.2.9 Ramjet sustain: combustor design considerations

In the conceptual design of a ramjet, one major consideration has to be done for the inlet throat. If the inlet throat area is relatively large, and a high-speed flow through the combustor is taken into account, this geometrical configuration may lead to low propulsion efficiency and to a lower specific impulse. At the other extreme, if the inlet throat area is relatively small, the mass flow might not be enough to provide the required thrust.

In the preliminary design, it has already been mentioned that a subsonic inlet is composed of a divergent section only. Furthermore, in the optimization cycle of the subsystem referring to the desired flight condition, the section area of the inlet is computed in order to guarantee the optimal mass flow rate necessary for the proper ramjet operation.

For cruise conditions, the following table is reporting the performed values of both cross section area of the inlet and mass flow rate.

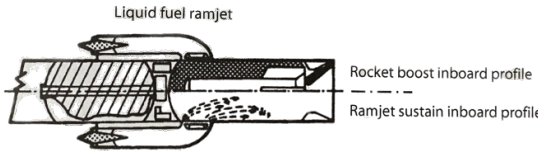


**Figure 3.6:** Integrated rocket ramjet configuration.

**Table 3.8:** Inlet integration

Inlet section area [m <sup>2</sup> ]	Mass flow rate [kg/s]
0.0299	112.01

### 3.2.10 Ramjet sustain: specific impulse, thrust prediction, and efficiency

As it can be seen from the equations for Table 3.9 and 3.10, the ideal specific impulse and thrust for a ramjet are a function of free stream Mach number  $M_0$ , heating value of fuel  $H_f$ , combustion temperature  $T_6$ , free stream temperature  $T_0$ , free stream flow area of the inlet  $A_0$ , free stream static pressure  $P_0$ , specific heat at constant pressure  $c_p$ , free stream speed of sound  $a_0$ , and free stream specific heat ratio  $\gamma_0$ . The necessary assumptions are: isentropic inlet and nozzle, low subsonic combustion with the combustor static temperature approximately equal to the combustor total temperature, constant combustion pressure, ideal expansion at the nozzle exit, and constant specific heat ratio  $\gamma = \gamma_0 = 1.4$ . Clearly, it is assumed that the ramjet combustor pressure is sufficiently high to provide complete combustion.

The specific impulse is computed for both acceleration and cruise phase, as reported in Table 3.9.

**Table 3.9:** Specific impulse.

$$\frac{I_s g_0 c_p T_0}{a_0 H_f} = \frac{M_0 \left( \sqrt{\frac{T_6}{T_0}} - 1 \right)}{\left[ 1 + \left( \frac{\gamma_0 - 1}{2} \right) M_0^2 \right] \left( \frac{T_6}{T_0} \right) - 1}$$

Phase	Specific impulse [s]
Acceleration	1440.2
Cruise	1186.4

The same procedure is performed for the thrust computation, reported in Table 3.10.

**Table 3.10:** Thrust.

$$\frac{T}{p_0 A_0} = \gamma_0 M_0^2 \left( \sqrt{\frac{T_6}{T_0}} - 1 \right)$$

Phase	Thrust [N]
Acceleration	22803
Cruise	12987

At the end of the propulsion subsystem process it is possible to compute the efficiency, evaluating the thermal, propulsive, and total indexes. The results are shown in Table 3.11.

$$\eta_p = 2 \left( \frac{v_0/v_{out}}{1 + v_0/v_{out}} \right), \quad \eta_{th} = \frac{\dot{m}_a (v_{out} - v)v + \frac{1}{2} \dot{m}_a (v_{out} - v)^2}{\dot{m}_f (\Delta H_c + \frac{1}{2} v^2)} \quad (3.12)$$

$$\eta_0 = \eta_{th} \eta_p \quad (3.13)$$

**Table 3.11:** Engine efficiency

Efficiency	$\eta_{th}$	$\eta_p$	$\eta_0$
Acceleration phase	14.29%	88.61%	12.66%
Cruise phase	20.83%	92.93%	19.36%

### 3.2.11 SRM booster: propellant choice

One of the objectives of a rocket motor is to provide sufficient velocity to meet the missile range, time-to-target, and manoeuvrability requirements. Solid propellant rocket motor will be considered for the propulsion conceptual design of the booster.

The increment of velocity  $\Delta v$ , provided by the rocket motor, is mainly related to propellant weight-to-missile total weight fraction ( $W_p/W_i$ ), and to the propellant specific impulse. As a first approximation, a reference propellant directory is considered in Fig. 3.7.

Type	I <sub>sp</sub> , specific impulse [s]	$\rho$ , density [lbm/in <sup>3</sup> ]	Burn rate @1000 psi [in/s]	Safety	Observables
-Min smoke. No Al fuel or AP oxidizer. Either composite with nitramine oxidizer (CL-20, ADN, HMX, RDX) or double base. Very low contrail ( $H_2O$ ).	- 220-255	- 0.055-0.062	⊖ 0.25-2.0	-	⊖
-Reduced smoke. No Al (binder fuel). AP oxidizer. Low contrail (HCl).	○ 250-260	○ 0.062	⊖ 0.1-1.5	○	○
-High smoke. Al fuel. AP oxidizer. High smoke ( $Al_2O_3$ ).	⊖ 260-265	⊖ 0.065	● 0.1-3.0	⊖	-
<span style="color: blue;">●</span> Superior <span style="color: gray;">⊖</span> Good <span style="color: gray;">○</span> Average <span style="color: gray;">-</span> Poor					

**Figure 3.7:** Typical solid propellants for missiles.

Since the observability of the missile is not an issue for the assigned mission scenario, it is possible to select the type of the propellant referring to the highest specific impulse. For this reason, aluminium-fuelled has to be regarded as the best choice for the boost phase.

The composition of the selected solid propellant is the following: 68 % ammonium perchlorate ( $NH_4ClO_4$ ), 18 % aluminium, 14 % HTPB. The aluminium percentage in the fuel is the maximum allowed for such chemical configuration of the propellant. The combustion reaction is computed through the Nasa CEA software, where the chamber pressure and the expansion ratio are chosen as, respectively, 80 and 10 bars. Furthermore, the equilibrium condition inside the nozzle has been imposed. The results are summarized in Table 3.12.

**Table 3.12:** Results from CEA code.

MM [g/mol]	T <sub>c</sub> [K]	$\gamma$	c <sub>p</sub> [kJ/kgK]	c <sup>*</sup> [m/s]	c <sub>f</sub>	I <sub>sp</sub> [s]
26.225	3414	1.1819	1.9499	1584.6	1.6270	263.7

As a reference for the conceptual design, there is a clear convergence between the specific impulse given by the software and the one suggested by the literature for a rich aluminium fuel propellant.

### 3.2.12 SRM booster: flight performance

Including the effect of the missile drag, the required  $\Delta v$ , which should be reached after the boost phase, increases. Moreover, the theoretical gravity contribution for the expected trajectory would give a positive concurrence for the missile acceleration phase. The maximum incremental velocity of a rocket is a function of the propellant weight fraction and the specific impulse. From Newton's second law, the necessary velocity increment is given by the following equation  $\Delta v = \Delta v_{mission} + \Delta v_{drag} - \Delta v_{gravity}$ , where  $\Delta v_{mission}$  is required to accelerate the missile from the helicopter speed to Mach 2.5. The drag and gravity contribution are computed considering a constant value, subsequently integrated over time.

### 3.2.13 SRM booster: nozzle dimensioning

The physics of the rocket motor consists in high temperature/high pressure combustion of the propellant, which produces gas flowing out of the combustion chamber and exiting through the nozzle into the atmosphere, thus producing thrust. The expansion process could be considered, in a first approximation, as near-isentropic.

The nozzle is composed by a first convergent part, where the subsonic gas flow, coming from the combustion chamber, is accelerating to be at sonic condition at the throat of the nozzle, and by a divergent part to develop additional kinetic energy, which provides further thrust.

For the convergent part of the nozzle, the ratio between the combustion chamber area and the nozzle throat area is selected to be equal to 10. Refer to appendix D.

The area of the combustor has been selected from the baseline in the first place, but some considerations on the insulation thickness and the nozzle diameter are done ex ante. The nozzle expansion ratio is chosen considering that the isentropic expansion should match the atmospheric pressure at sea-level conditions. The specific heat ratio of the gas flow is an output of the Nasa CEA software. Considering the expansion ratio and the nozzle throat area, the exit area of the nozzle is computed automatically.

**Table 3.13:** Nozzle estimation

$A_{cc}$ [m <sup>2</sup> ]	Contraction ratio	Nozzle $A_t$ [m <sup>2</sup> ]	Expansion ratio $\epsilon$	Nozzle exit area [m <sup>2</sup> ]	$\gamma$
0.1354	10	0.0135	10	0.1354	1.1819

Numerically solving the nozzle expansion ratio equation, which is:

$$\epsilon = \frac{\left(\frac{2}{\gamma+1}\right)^{\frac{1}{\gamma-1}} \sqrt{\frac{\gamma-1}{\gamma+1}}}{\left(\frac{P_e}{P_c}\right)^{\frac{1}{\gamma}} \sqrt{1 - \left(\frac{P_e}{P_c}\right)^{\frac{\gamma-1}{\gamma}}}}, \quad (3.14)$$

it is possible to determine the pressure at the exit of the nozzle.

The computed exit pressure is equal to 1.0541 bar. The external pressure in an altitude range between 0 and 1000 meters has a value of approximately 1 bar or less. This means that the missile has a slightly under-expanded nozzle, with the supersonic plume expanding outside the nozzle exit, very close to the optimal expansion.

To dimension the nozzle, the RAO approximation has been used. This method consists in using a parabola to approximate the outline of the nozzle, taking a conical nozzle as a reference with a half angle of 15°. The proportion between the length of the under-construction nozzle and the referring one (in this case is 100%) determines the initial and final parabola angles. For the convergent part, a half angle of 45° has been chosen as an easy reference value. The length of

the convergent and divergent part can be estimated at this point with a simple trigonometric relation.

**Table 3.14:** Nozzle dimensions

Convergent nozzle length [m]	Divergent nozzle length [m]	Total nozzle length [m]
0.1419	0.5297	0.6716

### 3.3 Weight

After the analysis of the propulsion system described before, all the elements necessary for the computation of the propellant masses, both solid and liquid, are known. In this section, the masses of all the other components of the missile will also be estimated, at first through fitting curves and relations from data collection, to obtain a preliminary approximation, and then with a more complex iterative process, to derive a more precise value.

A first simple estimation about the total mass at launch can be done starting from historical data charts of operative military missiles, which relate weight to dimensions:

$$W_L = \rho_{missile} ld^2,$$

where  $\rho_{missile}$  is the fitting value of the density, which is assumed as 1107.2 kg/m<sup>3</sup> (0.04 lb/in<sup>3</sup>). The values of length and diameter would be taken from the baseline, but, since in this mission the warhead is greater, for this computation they are slightly enlarged to 0.4 m, for diameter, and to 5.6 m, for total length, in order to obtain a more reasonable approximation. Substituting these values inside the relation, the resulting total mass at launch is 990 kg.

A similar estimation can be done also for the body structure weight over launch weight, which has a typical value of 22 %, and for propellant weight over total motor weight, which is about 72 %. At the end of this section, the aforementioned assessments will be compared with the final results of the computations.

#### 3.3.1 Warhead design

Initially, Baratol 76 [11] was selected to be the possible explosive, because its high density allows to have a more compact warhead. After various attempts, it was concluded that a 250 kg warhead is not compatible with the requirement of an helicopter-launched missile, since it leads to excessive weight and dimensions. The final choice has been to consider an explosive mass which has the equivalent heat of explosion of 250 kg of TNT, an equivalence commonly used for explosive warheads. For this reason, a new explosive is selected: the HBX-3 (High Blast Explosive), which has a TNT equivalence of 195% [12], higher than Baratol 76, thus reducing the mass of the warhead to 128.2 kg while maintaining the same explosive power.

If the HBX-3 is not acceptable because of its stability or volatile properties, any other explosive can be used, but the mass must be limited to 128.2 kg, and the different density will slightly change the dimensions of the warhead.

The choice of the warhead and its weight limitations must be rediscussed with the costumers, to evaluate if the mission requirements could be modified after the preliminary conceptual design of the missile. In any case, some considerations such as storability, explosive power, and fragmentation should be taken into account to ensure the fulfillment of the costumer requirements.

The warhead is modeled as a cylindrical semi-armour piercing fragmentation warhead, with a delayed base fuze to ensure that the explosion will happen inside the target.

### 3.3.2 Ramjet mass evaluation

In addition to the warhead, another contribution to the payload mass is the guidance system, which will be discussed in detail later, but has an estimated mass of 58.2 kg [1], which accounts also for the batteries and the electrical systems.

Starting from the results of the iteration process, the propellant mass flow rate is computed from the fuel-to-air ratio and air mass flow rate. Then, propellant mass can be easily found knowing the ramjet burning time, which is computed in Section 3.4. This value is then increased by 5 % to account for the ignition phase and for safety reasons, then, from the density of the propellant, the volume is computed. Again, another factor of 2 % is introduced to account for the possible propellant boil-off inside the tank. In this way, the final propellant volume is found.

At this point, the material choice is needed to design the minimum thickness of the tank. Teflon was chosen because it allows to achieve impermeable thin wall containment at minimum weight [5]. The yield tensile strength  $\sigma_{yield}$  is found to be about 27 MPa, but considering a derating factor of 15 %, it decreases to 23 MPa. From this value, the minimum thickness is obtained through the relation:

$$t_{min} = SF \frac{pr}{\sigma_{yield}}, \quad (3.15)$$

where  $r$  is the tank radius,  $p$  is the internal pressure, equal to the ambient pressure because the tank is not pressurized, and  $SF$  is the safety factor equal to 1.15. Since the value found with this equation is very small, it will be difficult to manufacture. For this reason, the final thickness was imposed to be 1 mm.

The mass of the inlet was taken from the baseline [1] as 46.72 kg, and then increased by 2 % to 47.65 kg, since the computations resulted in a higher length with respect to the baseline.

Another mass to be considered for the ramjet is related to the turbopump for the fuel pressurization. To obtain it, the following mass estimating relation has been used:

$$M_{pump} = A \left( \frac{P_{req}}{N_{rot}} \right)^b,$$

where  $A = 2.6$  and  $b = 0.6667$ , while  $N_{rot}$  has been imposed to 1500 rpm (157.08 rad/s), and the required power  $P_{req}$  can be obtained from the fuel mass flow rate and the pressure jump, which are already known. The operating principle of the turbopump is based on power extraction from a turbine, which is set in motion by bleed air coming from the inlet [6]; this implies that the inlet section will be slightly enlarged in a successive design phase. If the turbine results to be too heavy, the turbopump can be substituted with a different kind of pump in a later design phase.

The external structural mass is now considered. For the material choice, thermal resistance, mechanical properties, and density must be taken into account: a good trade-off is represented by a titanium alloy, which is also the baseline material, in this case TMETAL 35A CP(ASTM Grado 1) 99.1 Ti. Nevertheless, a steel alloy named 30HGSA/30KhGSA [7] was finally chosen to avoid structural issues, especially instability and bending. After some trials with different typical values, the thickness was imposed to be equal to 4 mm. This guess value will be then verified in the structural analysis.

From this value, the mass of the external structure related to the ramjet can be easily found.

The same thickness is considered for the nosecone, but in this case the material chosen is Zinc Sulfide [1], which is typically used for supersonic missile up to Mach 3. Since this part is one of the most subjected to loads, a deeper analysis should be done in a successive design phase to reinforce it from the structural view point.

The last mass to be considered is that of the wings, for which the most suitable material is the titanium alloy, as previously mentioned .

### 3.3.3 Booster mass evaluation

In order to evaluate the masses of the booster an iterative method is implemented. The starting point is a guess value of the structural ratio  $\epsilon_s$ , which is used to compute the propellant mass through an optimization algorithm described in the following section. Once the propellant mass is computed, it is used to derive the masses of the combustion chamber, the insulation, the nozzle and the external structure. At this point, the structural ratio can be evaluated again and compared to the guess solution.

#### Propellant mass optimization algorithm

The starting point of the algorithm is the delta velocity already computed in Section 3.2.12, together with the guess value of the structural ratio. Moreover, the mass of the ramjet could be considered as the payload mass for the boost phase. In addition, all the solid propellant properties have been previously reported, such as the specific impulse, computed with the CEA software. To minimize the mass ratio of the stage, the following cost function is optimized:

$$\Delta v_{tot} - I_{sp}g_0 \ln\left(\frac{\lambda I_{sp}g_0 - 1}{\lambda I_{sp}g_0 \epsilon}\right) = 0, \quad (3.16)$$

where  $\lambda$  is a Lagrange multiplier and the variable of the optimization from which it is possible to obtain the step mass. Hence, the structural mass thanks to  $\epsilon$ , and finally the propellant mass.

$$m = \frac{\lambda I_{sp}g_0 - 1}{\lambda I_{sp}g_0 \epsilon}, \quad m_{step} = \left(\frac{m - 1}{1 - \epsilon m}\right)m_{pay} \quad (3.17)$$

The next step is the grain configuration of the propellant. The overall density of the propellant is computed as:

$$\rho = \frac{\frac{\%_{Al}}{\rho_{Al}} + \frac{\%_{HTPB}}{\rho_{HTPB}} + \frac{\%_{AP}}{\rho_{AP}}}{\frac{\%_{Al}}{\rho_{Al}} + \frac{\%_{HTPB}}{\rho_{HTPB}} + \frac{\%_{AP}}{\rho_{AP}}} \quad (3.18)$$

while the burning rate is assumed to be  $7.62 \cdot 10^{-2}$  m/s, by literature reference [1].

It is now possible to compute the propellant mass flow rate as  $\dot{m} = p_c \frac{A_t}{C^*}$ . At this point it is possible to find the burning time of the booster as the ratio between the propellant mass and the propellant mass flow rate.

Then, from literature, one of the most used grain configuration for missiles is the star shape, which guarantees a neutral thrust profile and has a typical volumetric fraction equal to 0.8 [2]. The volume of the propellant is obtained starting from the propellant mass and density. Then, the internal volume of the combustion chamber is simply the volume of the propellant previously computed, divided by the volumetric fraction.

Once the grain is designed, the next step is to obtain the structural mass of the booster, that is mainly due to the insulation, combustion chamber, external structure, and nozzle. For the insulation, the selected material is a silicone elastomer (DC 93-104) capable of withstanding temperatures up to 3300°C for several minutes, usually used as protective coating in rocket motor and ramjet combustion chambers [8], with a thickness of  $t_{ins} = 12.7$  mm [9]. Knowing its density and considering a cylindrical shape, the mass is easily found.

For the combustion chamber, the material selected is the same Titanium alloy used for the external structure. The thickness is evaluated on the basis of the internal pressure with Eq. (3.15), as done for the tanks, with a safety factor  $SF$  of 1.15. For a cylindrical shape, the mass is obtained.

The external structural mass is computed as explained in Section 3.3.2, with a different value for the length.

Knowing the dimensions of the nozzle, imposing a mean thickness of 5mm and choosing a composite material (65% silica fiber fabric / 35% phenolic resin [10]), the mass of the nozzle can also be found.

With all the structural masses and the propellant mass, a new structural ratio can be computed and compared to the initial guess to find the error. The procedure is iterated with the new value of structural ratio until the error converges to zero.

Alongside with the mass, also the length of each component is obtained so that at the end of the procedure it can be verified if the sum corresponds to the total length of the missile. This verification corresponds to the control equation of another iterative cycle, which changes the initial chosen length, and consequently the diameter, in order to optimize it to fit the internal components.

### 3.3.4 Center of mass

For the computation of the center of mass, the missile is divided into 6 sections: nose, warhead, tank, pump, combustion chamber and nozzle. Each section is modeled as a cylinder, with its center of mass corresponding to the geometric center with the exception of the nose, which is modelled as a cone with the center of mass at 2/3 of its length. After the evaluation of the masses of each section, the position of the overall center of mass is computed as the average position of the one of each section, weighted for its mass.

The computation has been done in three different phases: at launch, at the beginning and at the end of the cruise phase. The positions of the center of gravity, starting from the nose, are found to be respectively 3.5194, 3.0937, and 3.1378 meters. From the stability point of view, the boost phase is certainly the worst condition.

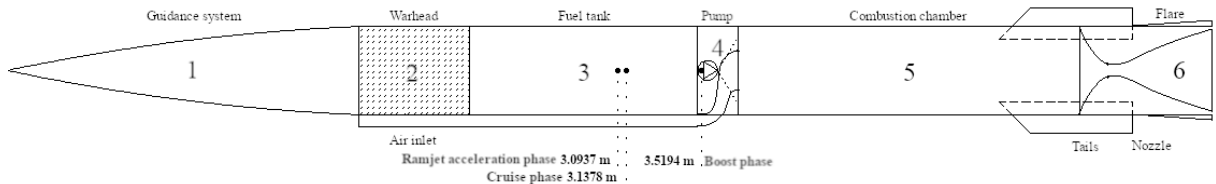


**Figure 3.8:** Different contributions to the center of mass.

## 3.4 Trajectory

For a generic launcher, at this point of the conceptual design, the aim would be to design a trajectory optimized for the time, aerodynamics, and fuel consumption point of view. It is important to notice, however, that for military missiles the mission priorities are different, since it is necessary to take into account that the missile could be intercepted and shot down during the flight and consequently it would not reach the target. To best prevent this eventuality, anti-ship missiles usually follow a sea skimming trajectory. This trajectory makes the detection of the missile more difficult because the missile appears over the horizon much later, delaying its identification from the enemy defense system.

For this mission, the missile is unhooked by the helicopter at 75 km from the target, and the solid booster is ignited after a very short free fall (5 m) for safety reasons. After ignition, a first manoeuvre is performed to insert the missile into a descending oblique trajectory that will take it at sea level altitude where, after a second manoeuvre, it will perform a sea skimming straight flight to the target. This second part is composed by an acceleration phase from M=2.5 to M=3, performed by the ramjet, and then a cruise phase at constant Mach number.

For the descending phase of the boost an iterative optimization cycle is performed in order to compute the angle of attack of the missile. An initial descending angle is selected as a guess

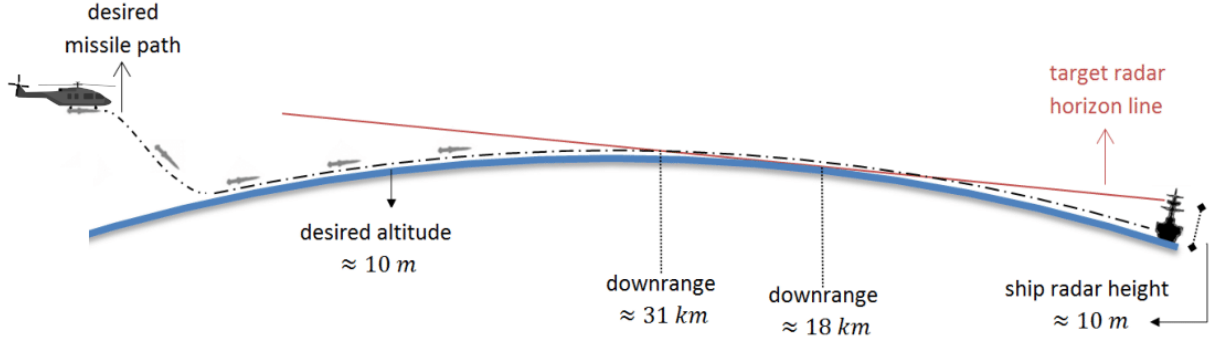


**Figure 3.9:** Typical sea skimming trajectory

**Table 3.15:** Manoeuvres data

Manoeuvre	Radius [m]	Maximum loading factor [g]
Free fall to booster	898	0.82
Booster to ramjet	940	78.5

for the cycle. With this value, the iterative process computes the corresponding range for the ramjet as the total range minus the horizontal component of the descent phase computed with the guess angle. At this point the ramjet and the booster are dimensioned. Then, a new descent angle is computed by imposing the time of flight of the first phase equal to the burning time of the solid propellant, to ensure that the descent phase is completed by the booster only.

The two phases are linked through an arc of circle manoeuvre, performed using the tails of the missile.

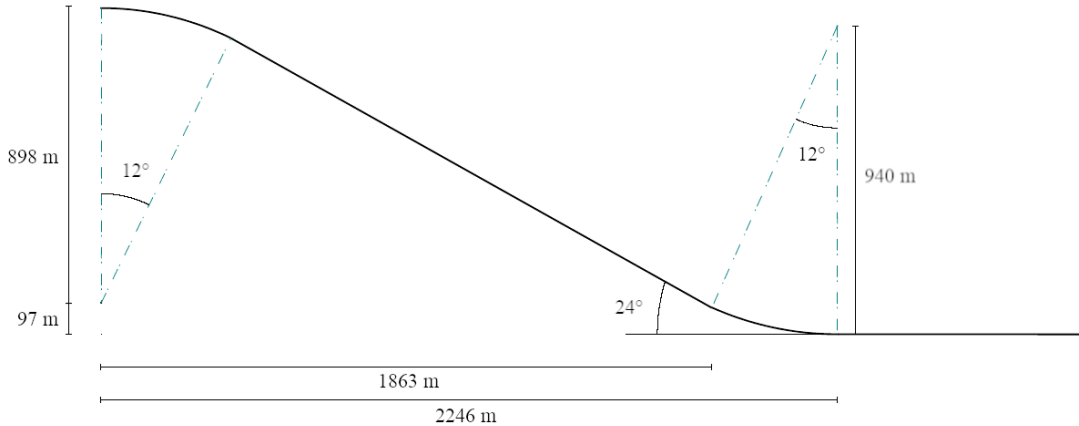


**Figure 3.10:** Detail of the two manoeuvres

### 3.4.1 Flight motion modelling

In 3 – *DoF* model, two aero-forces (normal, axial), and one aero-moment (pitching) are considered, together with the above mentioned thrust and weight forces. In this simulation, the pitching moment modelling includes the pitch stability and control derivatives, thus allowing a conceptual design sizing of the tail stabilizers. Moreover, this model is a good approach for the

initial analysis of a non-guided flight trajectory.

### 3.4.2 Guidance and control system

For the guidance and control system, a INS and GPS integrated system, which is a combination of a GPS-based system and an inertial platform, has been chosen and put inside the nosecone. This solution unites the long range accuracy of the GPS system with the sensibility to smaller corrections granted by the inertial platform. This coupled system can reach an accuracy up to 1 m for applications without an interference threat [13]. The addition of the INS also reduces the sensitivity to eventual GPS jamming near the target. Moreover, this system does not require windows for the sensors or particular shapes of the nosecone, like those required by radar-based systems and such, so the ogive can be made sleeker to be more adaptable for the low altitude high speed flight of the missile.

Since the target is big and slow it will not be able to perform evasive manoeuvres, so the guidance system will follow the estimated target position based on its latest coordinates, heading, and speed provided by the helicopter at the launch phase. If necessary, the target position can be updated during the flight with new information from the helicopter or from other friendly units nearby. However, it is still required that the target is already in the fire line of the missile at the moment of the launch.

Additionally, a small downward pointing radar could be added to check that the height in the sea skimming phase remains constant to lower the risk of collision with the surface of the sea.

## 3.5 Structural analysis

The main goal of this section is to determine the structural behavior of the system designed up to now. In order to do this, the results of aerodynamics, mass estimation, propulsion, and trajectory are necessary. After some considerations on the loads in different phases of the mission, the aerodynamic ones, acting on the missile in the solid rocket boost phase, turned out to be the most critical. For this reason they are taken into account in the structural analysis. To verify this hypothesis, the aerodynamic loads, with respect to the nose of the missile, have been computed. As it can be seen from F.1, the moments on the missile are not balanced, so this can induce a rotation of the missile. This could be corrected in a further design phase with the addition of a control system appendix G. In fact, in the ramjet cruise phase, the loads are negligible with respect to the first acceleration phase because of the smaller angle of attack. At the end of this evaluation, the effect of inertial loads in the acceleration phase and the aerodynamic moments in the second maneuver has also been verified, both resulting to be less critical, as expected.

### 3.5.1 External structure thickness

As previously stated in Section 3.3.2, the thickness of the external case has been imposed to be equal to 3 mm, but, after some trials, the first value that verifies the structural analysis was found to be 4 mm. To verify this hypothesis, the following equations were selected (from [1]):

- required thickness to counter localized buckling from bending:  $2.9 \frac{r\sigma_{bb}}{E}$
- required thickness to counter localized buckling from axial compression:  $4 \frac{r\sigma_{ba}}{E}$
- required thickness to accommodate a thrust force load:  $\frac{T}{2\pi\sigma_{yield}r}$
- required thickness to accommodate a bending moment load:  $\frac{m_b}{\pi\sigma_{yield}r^2}$

where the buckling bending stress  $\sigma_{bb}$  and the buckling axial stress  $\sigma_{ba}$  are taken equal to the yield stress  $\sigma_{yield}$  of the steel. To choose the final value, the maximum thickness from the

previous formulas is taken and multiplied by a safety factor, to match the initial guess of 4 mm. This validation criterion is the least conservative and was selected for weight reasons, in order to guarantee the compatibility with the launch platform.

### 3.5.2 Frequency analysis

Once the thickness of the external structure is evaluated, it is possible to determine the first bending frequency of the missile, under the assumptions of the body as a free-free beam with a hollow cylinder shape, as:

$$f_1 = \frac{9.87}{2\pi} \sqrt{\frac{\pi Et}{8M_s(\frac{l}{d})^3}}$$

For the value of thickness  $t$ , structural mass  $M_s$ , and fineness ratio  $l/d$  specified in the previous sections, the first bending frequency results to be 60.5 Hz. Considering an actuator frequency of the flight control system of 16 Hz, the margin is quite high and grants to avoid resonance issues, even for a smaller value of thickness. Fig F.2 in the appendix shows the relation between thickness and first bending frequency.

### 3.5.3 Compatibility with the helicopter

From the final results, the missile is bigger and heavier than any other payload currently carried by the Seahawk SH-60b, but still within the maximum load capability of the helicopter. So, it will need a new pylon, and its design is outlined in appendix E. In order to verify that the missile can be safely attached to the support, the static bending moment on the ground has been computed. The external structure of the missile is able to sustain these bending loads (see appendix E), but an internal reinforcement should be applied in correspondence of the attachment to support the shear loads. This can be done in a successive phase of the design.

For the release system of the missile it was chosen the Pneumatic Bomb Ejection Rack from COBHAM E.2, which is an ejection stroke system chosen for the compatibility with the missile. In fact, a rail system can not work with a long missile with flares, and it would be less safe. The risk to damage the helicopter in case of explosive failure of the booster is reduced, because the missile is ignited after the release.

## 3.6 Monte Carlo simulation

The Monte Carlo method allows a deeper check on the real application of the project results. Even if all requirements are respected theoretically, there still might be some uncertainties, coming from the variables that are not into the model of the conceptual design. Some of them would have random amounts. Therefore, it is possible to analyze their effects taking into account the mean values and a statistical distribution for the desired data, including the standard deviation of the population data itself.

In particular, two uncertainties, that will be part of the study, are the wind magnitude and the missile mass variation. The analysis has been performed considering a balance of forces, but not one of moments. This is because the wings of the missile are supposed to not change their angle of attack, therefore, once again, an active control system on the trajectory has been implemented. For instance, the test target is considered to be at the center of a tank ship anchored off coast, which has a length of 300m, and height of 50m.

### 3.6.1 Wind

The data regarding the wind magnitude have been retrieved from an online platform [15]. From here, it is possible to select a certain spot on the world surface, which in this case is on the

Mediterranean Sea, off shore of the coast of Tel Aviv. The reason for this choice is identified in the fact that the selected area presents a quite calm sea, so the probability of high waves is relatively low, general fair atmospheric conditions, for the helicopter flight limits, and a good weather station to effectively retrieve a database. The data corresponds to a time span of 4 years, from 2016 to 2020, considering gusts at 50 meters above mean sea level. Then, magnitude and wind direction are used to implement on *Matlab* a basic statistical population, to associate a normal probability distribution, and to retrieve the mean value  $v_{wind,mean} = 0.282\text{m/s}$ , and the standard deviation of the data itself  $\sigma = 2.7921\text{m/s}$ . The wind effects are considered on the perpendicular direction only, with respect to the one of the missile trajectory. In addition, just the last 15 seconds of the missile path has been considered.

The success rate is 21.2%, in fact a missile with no guidance systems will very likely miss its target, even for small variations in the trajectory due to wind gusts. The range of success is considered to be  $\pm 149\text{m}$ , choosing to consider that a non significant damage occurs if the edges of the ship are hit. Therefore, a simplified control system, hinted in appendix G, is able to mitigate the effects on trajectory perturbations, making the missile much more accurate and reliable.

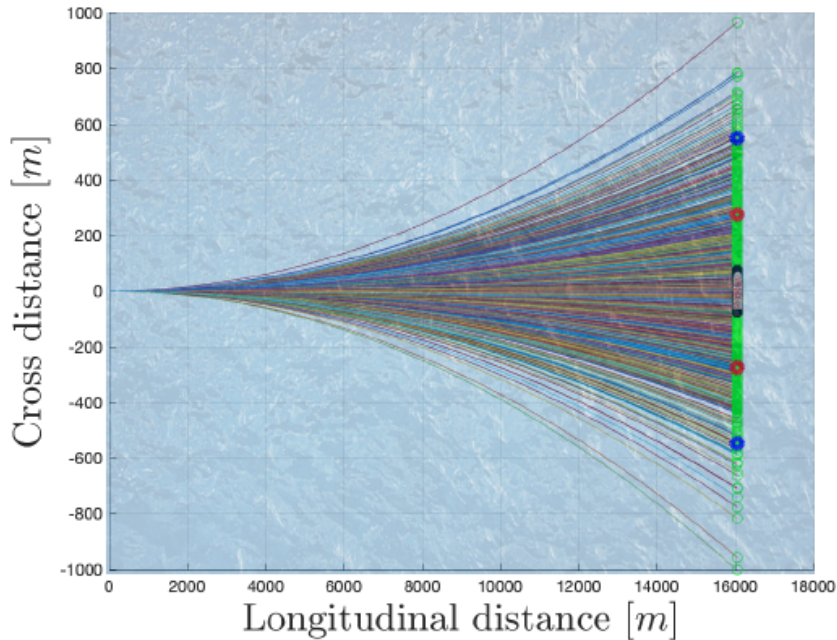


**Figure 3.11:** Monte Carlo simulation with wind perturbation. 1000 trajectories outlined, between red markers are 68% trajectories with a standard deviation of 274.4073m, between blue markers are 97% trajectories with a standard deviation of 548.8146m. The target is at the centre.

### 3.6.2 Missile Mass

Another parameter which has been considered is the total mass of the missile. This choice has been done because, in a preliminary design phase, the mass may need to be changed due to some late variations in the design process. Hence, it is a good procedure to verify that the mission requirements are still respected, if such possibility occurs. For this analysis, the nominal mass of the missile has been taken to be the mean value, and a standard deviation of 20 kg has been hypothesized.

$$Y = \frac{1}{m}[F_{body} + F_{tail}] \frac{t^2}{2}, \quad (3.19)$$

where  $Y$  is the drift caused by the wind,  $F_{body}$  is the force acting on the body,  $F_{tail}$  is the force acting on the tail, and  $t$  is time.

Mass does not change much the results, and the dominant parameter is still the wind factor. From a stability point of view, a final compromise is analyzed in order to perform a global optimization of the missile. Clearly, from the initial considerations done in the House of Quality, the mass of the missile is the most critical parameter. The aim of the whole project is to obtain a final mass which could be compatible with the launch platform. This remains the focus of the workflow, but a greater mass would make the missile less subject to wind perturbations, and on the other hand a lighter missile is more sensitive to gusts. Since this compromise could not be solved uniquely, the optimal choice to have a limit mass, and a functional trajectory, is to implement a dynamic control system capable to matching the targets.

### 3.7 Final considerations on stability

Before the end of the first phase of design, some considerations can be done about aerodynamic stability. To do so, the evaluation of the center of gravity, derived from the weight analysis, is fundamental. Then, the center of pressure can be computed: if it is behind the center of gravity, the missile will be stable, otherwise it will be unstable.

From an aerodynamic point of view, the initial descent phase performed by the booster is the most critical stage of the mission in terms of stability. In the idea of conceptual design, the most convenient choice that could be done for a preliminary aerodynamic optimization is to add a small flare at the end of the missile, in order to achieve a global stability. In fact, if the descending phase is analyzed without designing a flare, problems in stability should occur creating a very difficult matching of the two expected trajectories for the mission scenario. In appendix I, the computations are plotted for the configuration without flare: it is clearly an unstable condition which could be critical during the acceleration descending phase. In Fig 3.12 and 3.13, instead, it is reported the plot with a small flare designed for the missile. From this plot, it is possible to conclude that even though a stable configuration is not completely achieved, the overall aerodynamic configuration of the missile is optimized. Moreover, in the figure, the position of center of pressure is performed according to the initial analysis done in the aerodynamic subsystem of the conceptual design.

The same procedure is established for the cruise phase of the ramjet at Mach 3. In this part of the trajectory a stable condition is guaranteed by the evaluation of the position of both center of gravity and center of pressure.

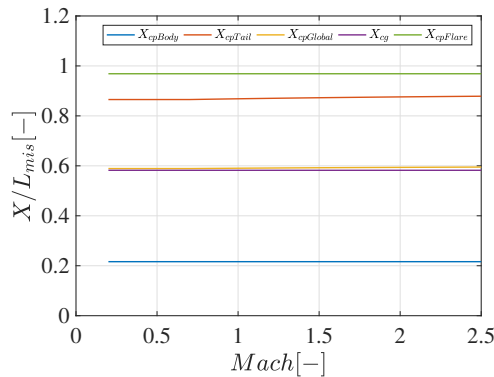


**Figure 3.12:** Descending phase

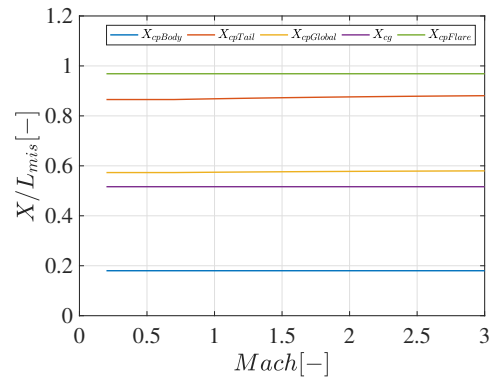


**Figure 3.13:** Cruise phase

Clearly, the final decision to design a small flare for stability issues must be followed by a shift of 40 cm forward for tails.

# Chapter 4

## Concluding remarks

At the end of the conceptual design, the missile complies with all the requirements set by the customer leaving the discussion about the explosive still open, with the two alternatives of the TNT equivalence with HBX-3, or the weight reduction of the warhead mass keeping Baratol 76. Relying on the data about the warheads of already existing anti-ship missiles, which in some cases carry an amount of explosive even lower than in the reduced Baratol 76 case, it is possible to state that both options would achieve the destruction of the target. It is however likely that successive iterations in the design process will allow a further reduction of the total mass, opening the possibility of keeping the original warhead.

The weight and the dimensions of the *Sea Harvester* allow the SH-60 to carry two missiles (one on each side) thanks to a specifically designed support (appendix E), which gives the helicopter an advantage in balance during flight and the possibility of a second shot in case of failure of the first one.

The choice of Zinc Sulfide for the nose allows changes to the guidance system in case a more precise identification of the target is needed, since this material is compatible with radars. In conclusion, even if the current design already fulfills the customer requirements, it deliberately leaves space for changes in order to match eventual future needs or strategic decisions.

**Table 4.1:** Final result of preliminary design

Total length	6.228 m
External diameter	0.445 m
Total mass	1065.8 kg
Booster propellant mass	329.979 kg
Ramjet propellant mass	149.43 kg
Total range	75 km
Boost phase length	2465 m
Acceleration phase length	14549 m
Cruise phase length	58198 m
Boost time	4.829 s
Acceleration time	15.549 s
Cruise time	57.013 s
$C_L$ during cruise	0.0691
$C_D$ during cruise	0.1099

# Bibliography

- [1] E.L. Fleeman, J.A. Schetz, *Missile Design and System Engineering*, "AIAA education series", American Institute of Aeronautics and Astronautics, 2012
- [2] G.P. Sutton, O. Biblarz, *Rocket Propulsion Elements*, "A Wiley Interscience publication", Wiley, 2001
- [3] L. G. De Grace, The Bendix Corporation *Development of a spark ignition system for a ramjet missile*, Journal of Spacecraft and Rockets, São José dos Campos, Vol. 5, No 11, Nov., 1968
- [4] ADVISORY GROUP FOR AEROSPACE RESEARCH AND DEVELOPMENT, *Ramjet and Ramrocket Propulsion Systems for Missiles*, Defense Technical Information Center, Sep. 1984
- [5] Holscot Industrial Linings, *Liquid rocket fuel tanks of Teflon*, Anti-Corrosion Methods and Materials Vol. 47 Issue 6, Dec. 2000
- [6] Joel D. Peterson, *Air-fuel ratio control system for ram-jet engines*, US Patent 2,765,619, patented Oct. 9, 1956
- [7] <http://www.ausairpower.net/APA-Rus-ASM.html>
- [8] <https://www.eis-inc.com/ablative-material/p-dc93-104x11lb/specifications-0/Dow-Corning-93-104-Ablative-Material,-5kg-Kit,-Colorless-Black-Technical-Data-Sheet>
- [9] Donald A. Wiederecht, Robert V. Williams, *Integral ramjet booster demonstration program*, Lockheed Propulsion Company, February 1975, p. 63
- [10] Homero P. Silva, Luiz C. Pardini, Edison Bittencourt *Shear Properties of Carbon Fiber/Phenolic Resin Composites Heat Treated at High Temperatures*, J. Aerosp. Technol. Manag., São José dos Campos, Vol. 8, No 3, pp.363-372, Jul.-Sep., 2016
- [11] T.R. Gibbs, A. Popolato, J.F. Baytos, *LASL Explosive Property Data*, "Los Alamos Scientific Laboratory Serie Son Dynamic Material Properties, Vol 4", University of California Press, 1980
- [12] Paul W. Cooper, *Comments on TNT equivalence*, Presented at the 20th International Pyrotechnics Seminar Colorado Springs, Colorado July 24-29, 1994
- [13] George T. Schmidt, *Navigation Sensors and Systems in GNSS Degraded and Denied Environments*, NATO educational notes, STO-EN-SET-197
- [14] <https://www.cobhammissionsystems.com/weapons-carriage-and-release/air-to-ground-weapons-carriage-and-release-systems/air-to-ground-bomb-racks/pneumatic-bomb-ejection-rack-pber-datasheet/docview/>
- [15] Wind Data Retriving: [http://mesonet.agron.iastate.edu/request/download.phtml?network=IL\\_\\_ASOS](http://mesonet.agron.iastate.edu/request/download.phtml?network=IL__ASOS)

[16] <https://info.publicintelligence.net/USNavy-SH60.pdf>

## Appendix A

# House of Quality and Risk Matrix

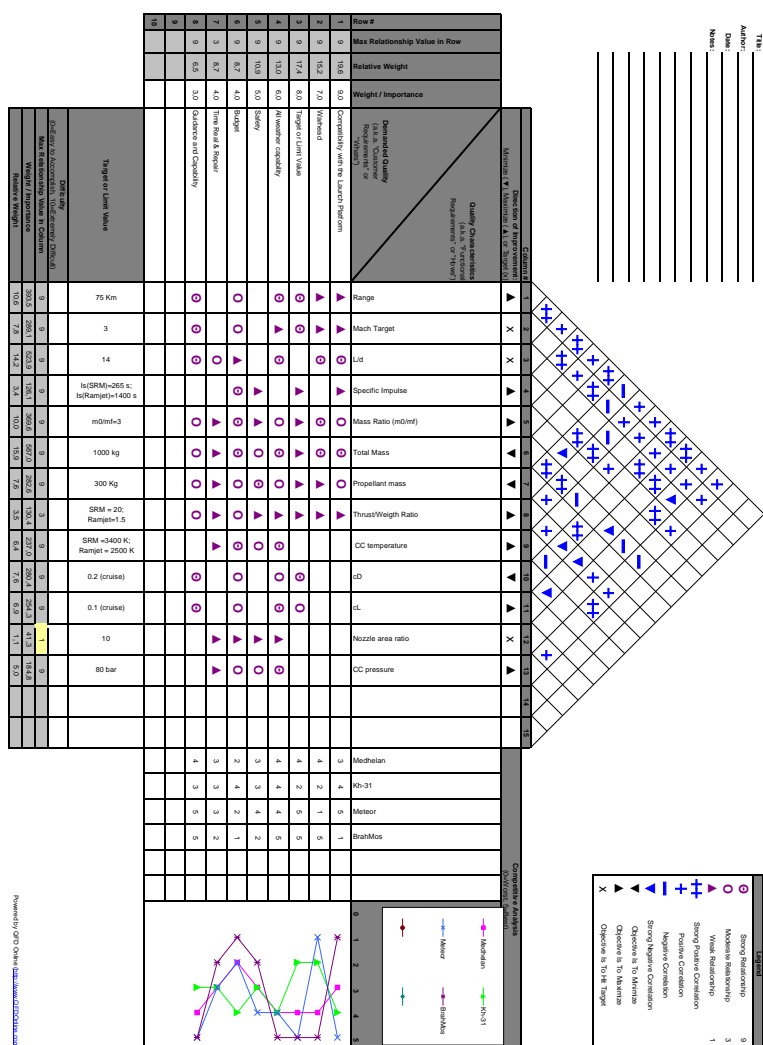


Figure A.1: House of Quality of the project.

## Appendix B

### Helicopter data

Helicopter data are taken from [16].



**Figure B.1:** Launch platform is the helicopter SH-60 of the US navy.

**Table B.1:** Main SH-60 data.

Overall length	19.76 m
Height	5.18 m
Empty weight	6895 kg
Max takeoff weight	10433 kg
Altitude at launch	1000 m
Cruise speed	270 km/h
Max range	834 km
Max ceiling	3580 m

## Appendix C

# Isentropic flow and Shock Waves

$$M = \frac{v}{\sqrt{\gamma RT}} \quad (\text{C.1})$$

$$\frac{p}{p_t} = \left(1 + \frac{\gamma - 1}{2} M^2\right)^{\frac{1}{1-\gamma}}, \quad \frac{T}{T_t} = \left(1 + \frac{\gamma - 1}{2} M^2\right)^{-1}, \quad \frac{\rho}{\rho_t} = \left(1 + \frac{\gamma - 1}{2} M^2\right)^{\frac{1}{1-\gamma}} \quad (\text{C.2})$$

$$\frac{A}{A^*} = \left(\frac{\gamma - 1}{2}\right)^{\frac{-\gamma+1}{2(\gamma-1)}} \frac{\left(1 + \frac{\gamma-1}{2} M^2\right)^{\frac{\gamma+1}{2(\gamma-1)}}}{M} \quad (\text{C.3})$$

Where  $-t$  is referring to total conditions,  $*$  is referring to sonic conditions.

**Table C.1:** Rayleigh combustion in cruise phase

f/a=0.0165	Mach number	Static temperature	Static pressure
Combustor exit	$M_6=0.059$	$T_6=1450.2 \text{ K}$	$P_6=76.57 \cdot 10^5 \text{ Pa}$
Combustor entry	$M_5=0.044$	$T_5=806.51 \text{ K}$	$P_5=76.57 \cdot 10^5 \text{ Pa}$

**Table C.2:** Shock conditions at Mach 2.5-3

Shock wave	Upstream Mach	Downstream Mach	Upstream static pressure [Pa]	Downstream static pressure [Pa]	Upstream static temperature [K]	Downstream static temperature [K]
Oblique 1	$M_0=2.5$	$M_1=1.92$	$P_0=101325$	$P_1=3.2 \cdot 10^5$	$T_0=288.15$	$T_1=417.56$
Oblique 2	$M_1=1.92$	$M_2=1.43$	$P_1=3.2 \cdot 10^5$	$P_2=6.35 \cdot 10^5$	$T_1=417.56$	$T_2=512.84$
Oblique 3	$M_2=1.43$	$M_3=1.26$	$P_2=6.35 \cdot 10^5$	$P_3=8.04 \cdot 10^5$	$T_2=512.84$	$T_3=548.96$
Normal	$M_3=1.26$	$M_4=0.81$	$P_3=8.04 \cdot 10^5$	$P_4=1.36 \cdot 10^6$	$T_3=548.96$	$T_4=640.79$

**Table C.3:** Shock conditions at Mach 3

Shock wave	Upstream Mach	Downstream Mach	Upstream static pressure [Pa]	Downstream static pressure [Pa]	Upstream static temperature [K]	Downstream static temperature [K]
Oblique 1	$M_0=3$	$M_1=2.09$	$P_0=101325$	$P_1=3.45 \cdot 10^5$	$T_0=288.15$	$T_1=430.72$
Oblique 2	$M_1=2.09$	$M_2=1.59$	$P_1=3.45 \cdot 10^5$	$P_2=7.08 \cdot 10^5$	$T_1=430.72$	$T_2=534.48$
Oblique 3	$M_2=1.59$	$M_3=1.43$	$P_2=7.08 \cdot 10^5$	$P_3=8.97 \cdot 10^5$	$T_2=534.48$	$T_3=572.15$
Normal	$M_3=1.43$	$M_4=0.73$	$P_3=8.97 \cdot 10^5$	$P_4=1.99 \cdot 10^6$	$T_3=572.15$	$T_4=729.76$

## Appendix D

### Nozzle contraction ratio

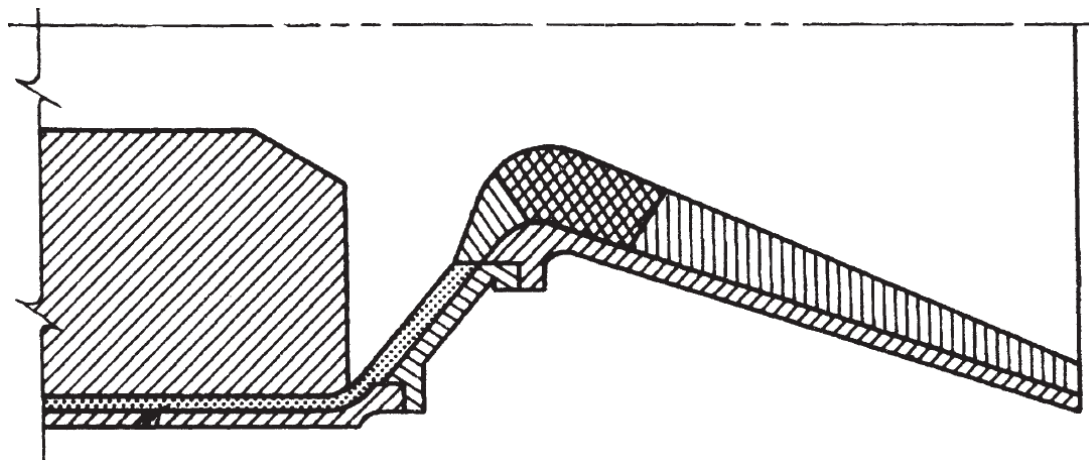


**Figure D.1:** Booster nozzle

For solid rocket motors, it is possible to use the Fig. D.1 as a reference to dimension the nozzle considering its exit and throat area, with the combustion chamber area. Selecting an expansion ratio equal to 10, to match the external pressure during the mission scenario, the focus of the problem is related to the contraction ratio. Since solid rocket boosters have bigger combustion chambers, with respect to liquid engines due to the necessity to contain the propellant grain, the contraction ratio will be higher, up to the point where it could be approximately equal to the expansion ratio. This consideration justifies the area ratios selected during the propulsion preliminary design process.

## Appendix E

# Pylon preliminary design

Regarding the choice of the pylon, a zero lift profile was considered to reduce drag. The internal structure is made of an HEM 100 shaped spar, with two ribs. The section is the more conservative to support bending loads. The total weight is 10 kg and the length is 70 cm, in order to avoid interference with other components of the helicopter, and is made of ergal (series 7000 aluminum). The pylon is verified to withstand a bending load of 4 tons.

The new pylon could be attached in place of the already existing ordnance hardpoints on the sides of the helicopter, where the capability to sustain loads is greater, on both sides. Another option could be to utilize braced pylon attached behind the cockpit as shown in figure below, but only one missile can be attached for each pylon.



**Figure E.1:** Render UH60-BlackHawk.

## PBER

Pneumatic Bomb Ejection Rack

**COBHAM**

### Smart Design, Smart Solution

The PBER rack was designed as a pneumatic replacement with the same form, fit and function as the MAU-12. Designed and integrated initially on the F-10 Block 60, the PBER rack is a fully pneumatic rack capable of carrying and releasing stores of up to 2,882 lb (1,307 kg). The PBER also has unique design features not offered by other bomb racks which allow larger stores to be carried in closer proximity to other stores on an aircraft, allowing for greater mission flexibility.

### Cost Savings

As with all pneumatic racks one of the main benefits is the cost savings when comparing to older pyrotechnic racks. The PBER offers clean, reliable and safe pneumatic ejection of stores from fast jet aircraft. The PBER is designed around the existing MAU-12 bomb rack which significantly reduces integration costs as there is no need for pylon modifications. PBER is also a ground fill type pneumatic rack which means that no additional hardware is required on the aircraft.

### Unique Features and Benefits

The PBER utilizes pneumatic ejection technology which ejects the stores using compressed air as opposed to older systems which rely on pyrotechnic cartridges. This requires significantly less logistical support, maintenance and repair than legacy systems and as a result the total cost of ownership is greatly reduced.

### Key Features

- Fully constrained release
- 6.35" (161 mm) ejection stroke
- Physical interface identical to a MAU-12
- 14" (356 mm) and 30" (762 mm) hook centers
- 10.7" (272 mm) to 30" (762 mm) store diameter capability
- Reduced maintenance and cleaning

### Specifications

Payload Capacity	Single stores up to 2,337 lb to 2,882 lb (1,000 kg) to (1,307 kg)
Weight	90 lb (44 kg)
Dimensions	30" x 3" x 8" (915 mm x 77 mm x 204 mm)

### Platform Integration

Currently integrated on the F-10 Block 60. Can easily be integrated on to other F-10 or other platforms, such as the A-10.

### Performance

EOS Velocity	Up to 18 ft/s
--------------	---------------



PBER Pneumatic Bomb Ejection Rack

For further information please contact:

**Cobham Mission Systems**  
10 Cobham Drive  
Orchard Park, NY 14217 USA

Tel: +1 (716) 662 0000  
Fax: +1 (716) 662 0747

© Cobham plc, 2009

Cobham Technologies, Inc. is acting solely as Cobham Mission Systems. The information contained herein does not represent legal advice. It is intended for guidance only. It should not be used for specific decisions or warranty, liability or implied warranties or express source information.

[www.cobham.com/missionsystems](http://www.cobham.com/missionsystems)

**Figure E.2:** Pneumatic Bomb Ejection Rack

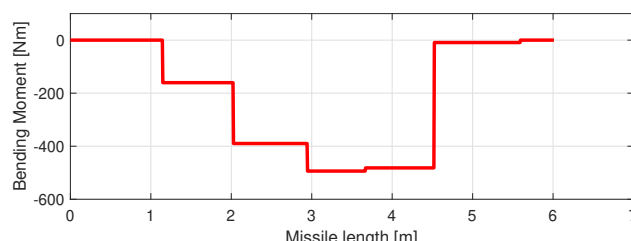


**Figure E.3:** Static bending moment calculated on ground.

## Appendix F

# Structural Analysis

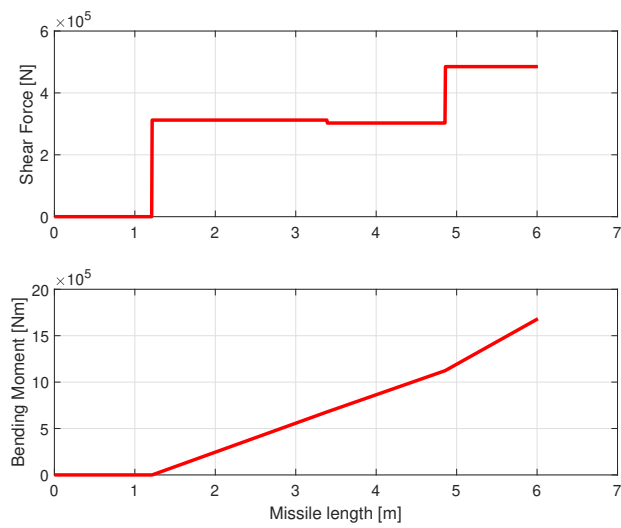


**Figure F.1:** Shear forces and bending moment with respect to the nosecone during boost phase.

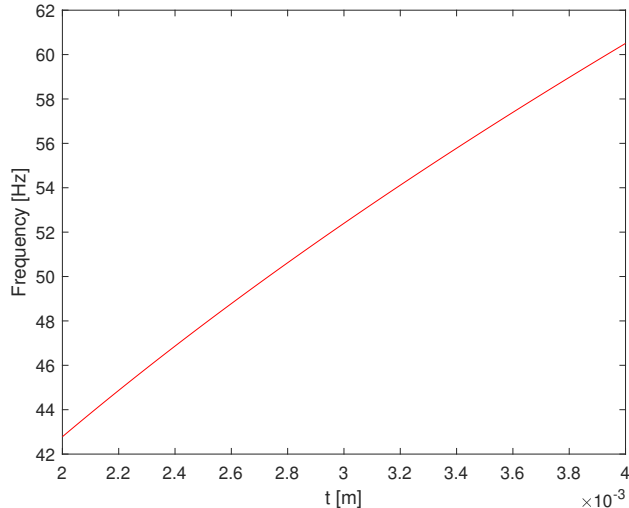


**Figure F.2:** First bending frequency for different values of thickness.

## Appendix G

# Theoretical analysis on a possible control system

A control system would provide the missile an improved stability, if significant external factors are encountered, and a better accuracy, increasing the chances to hit the target.

In this case, the control block diagram shown below is capable to attenuate lateral perturbations, implying that the missile should fly in straight trajectory to hit the target. Therefore, no control is possible if the initial release of the missile is not on the target fire line.

The error on the trajectory is computed considering the difference between the desired angle  $\phi_0$  and the attitude yaw angle  $\phi$ , with a closed feedback loop. The system implemented is a MIMO system, with  $\delta_{lat}$  as input,  $\phi$  and  $p$  as outputs.  $\delta_{lat}$  is the deflection angle of the tail which changes the yaw angle  $\phi$ , and the angular velocity  $p$  around the yaw axis itself. A PI controller would be able to strongly respond to lateral trajectory variations, with the proportional part, and to attenuate the angular speed on the yaw angle with the integrative part, thus fulfilling the exemplified task. The controllers are  $R_\phi$  and  $R_p$ . A block diagram is shown in Fig. G.1.

$$\begin{bmatrix} m & 0 & 0 & 0 & 0 \\ 0 & I_x & -I_{xz} & 0 & 0 \\ 0 & -I_{xz} & I_z & 0 & 0 \\ 0 & 0 & 0 & 1 & 0 \\ 0 & 0 & 0 & 0 & 1 \end{bmatrix} \begin{bmatrix} \dot{v} \\ \dot{p} \\ \dot{r} \\ \dot{\varphi} \\ \dot{\psi} \end{bmatrix} + \begin{bmatrix} -\tilde{Y}_v & -(\tilde{Y}_p + mW_e) & -(\tilde{Y}_r - mU_e) & -mg \cos \theta_e & -mg \sin \theta_e \\ -\tilde{L}_v & -\tilde{L}_p & -\tilde{L}_r & 0 & 0 \\ -\tilde{N}_v & -\tilde{N}_p & -\tilde{N}_r & 0 & 0 \\ 0 & -1 & 0 & 0 & 0 \\ 0 & 0 & -1 & 0 & 0 \end{bmatrix} \begin{bmatrix} v \\ p \\ r \\ \varphi \\ \psi \end{bmatrix} = \begin{bmatrix} \tilde{Y}_{\delta_{lat}} \\ \tilde{L}_{\delta_{lat}} \\ \tilde{N}_{\delta_{lat}} \\ 0 \\ 0 \end{bmatrix} [\delta_{lat}] \quad (G.1)$$

Where:

- $m$ : mass of the missile;
- $I_x, I_z, I_{xz}, I_{zx}$  : moments of inertia;
- $\tilde{Y}_v, \tilde{Y}_p, \tilde{Y}_r, \tilde{L}_v, \tilde{L}_p, \tilde{L}_r, \tilde{N}_v, \tilde{N}_p, \tilde{N}_r$  : aerodynamic stability derivatives;
- $\tilde{Y}_{\delta_{lat}}, \tilde{L}_{\delta_{lat}}, \tilde{N}_{\delta_{lat}}$ : control stability derivatives.

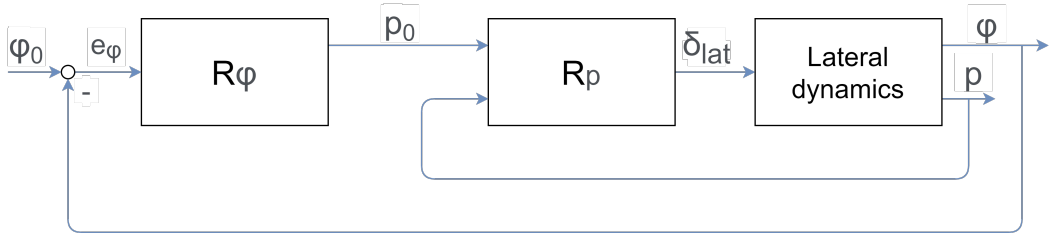
Eq.(G.1), is the general equation of the lateral motion of the missile written in the following shape:

$$M\dot{x}(t) + Kx(t) = Fu(t) \quad (G.2)$$

If equation (G.2) is "divided" by  $M$ , the following matrices can be defined as  $A = -M^{-1}K$  and  $B = M^{-1}F$ . Hence, the state space model equations are obtained, and they can be written in the following form:

$$\dot{x}(t) = Ax(t) + Bu(t) \quad (G.3)$$

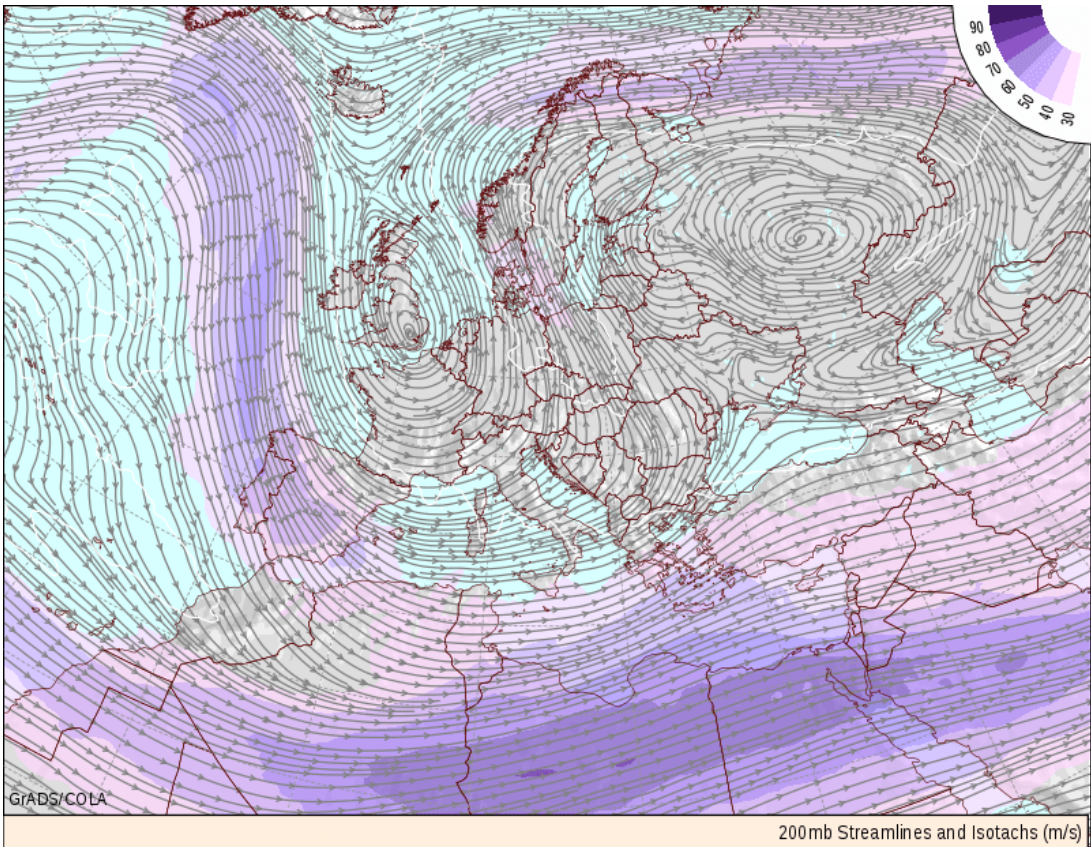
Once the aerodynamic and control stability derivatives are determined, the state space can be solved. Retrieving data from a dynamic simulation, it is possible to determine the tunable parameters of the two controllers. Then, it is possible to implement the state space form of the system in Matlab, tuning the controllers with the integrated function *systune*. Hence, it is possible to decide the overshoot, time constant, and order of the frequency response. Once the controllers are tuned, an uncertainty analysis, to verify the closed loop feedback system stability, should be performed. It is possible to integrate the so called "*M – Δ analysis*" and the "*μ – analysis*" with the structured singular values, to verify the static and robust stability of the system. A further Monte Carlo simulation could be implemented to verify the control system with possible variations of the input and control parameters in a real application.



**Figure G.1:** Block diagram of the control system

# Appendix H

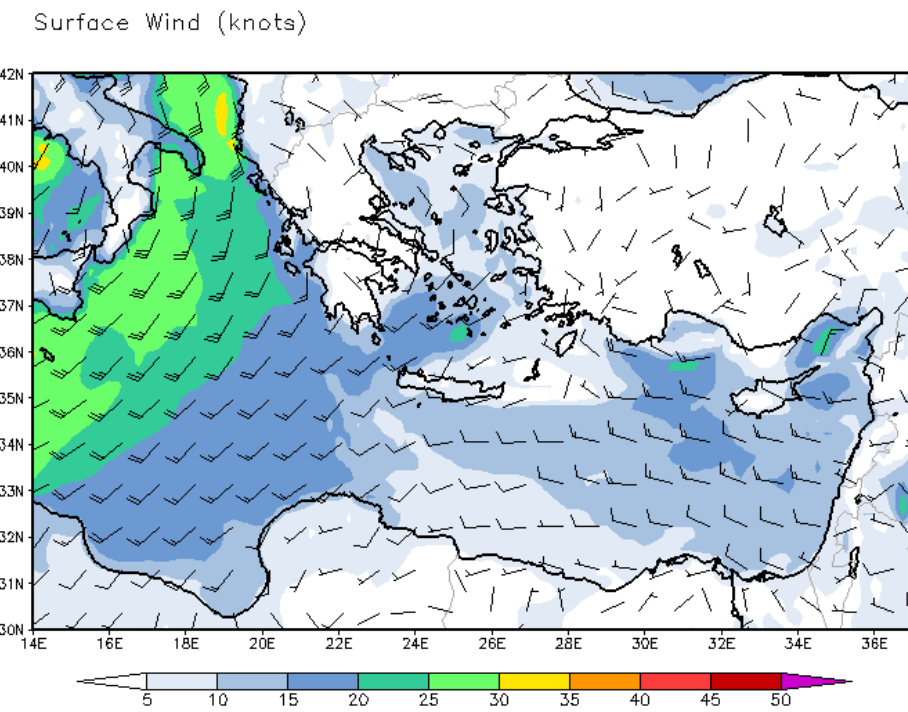
## Meteograms



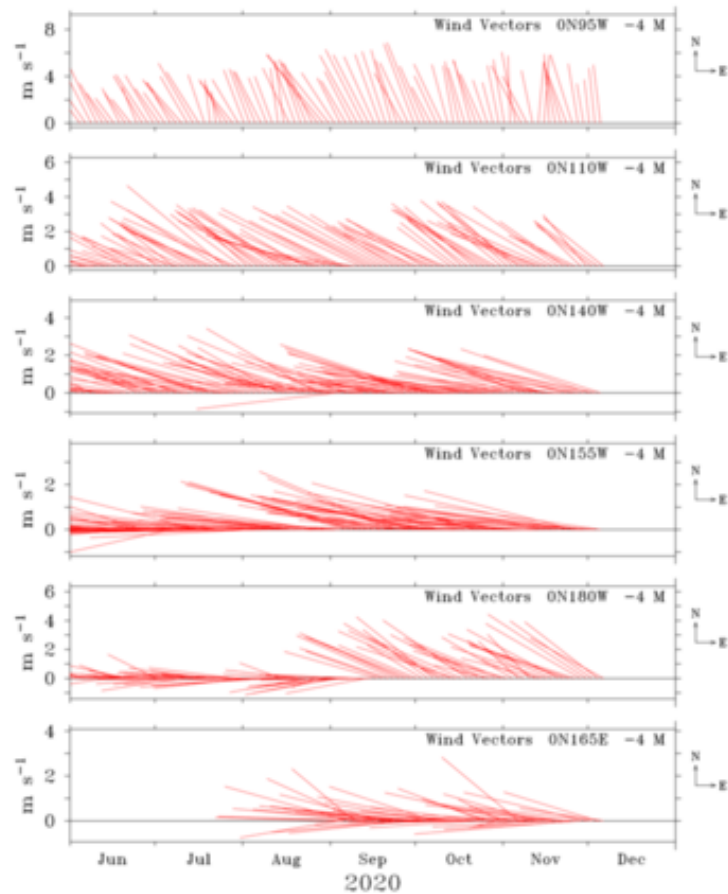
**Figure H.1:** Typical Europe Wind Chart

Fig. H.1 shows generic wind isotachs streamlines, in ambient pressure of 200mb. It is possible to see the mass of air generally moving in the region of the chosen target: warm fronts usually coming from the African Continent, colliding with cold fronts coming from Continental Europe, combined with rainy air coming from the Atlantic Ocean. This creates a recirculation zone which causes a good scenario for testing the missile guidance performances in the Monte Carlo simulation: usually calm sea, with low waves, and typically NE winds with moderate speed.

Fig. H.3 shows the wind vectors, considering N-E as the positive directions. In the different graphs, time is changing in 24h, at intervals of 2 hours, starting from midnight. Moreover, the magnitude of the wind is represented by the length of the vector. It is possible to see that the majority of the wind streams are directed eastward throughout the year. This is just a visual representation of a portion of data actually used in the Monte Carlo analysis.



**Figure H.2:** Detailed wind direction in the Mediterranean target location



**Figure H.3:** Wind vectors from Jun to Dec 2020

# Appendix I

## Stability

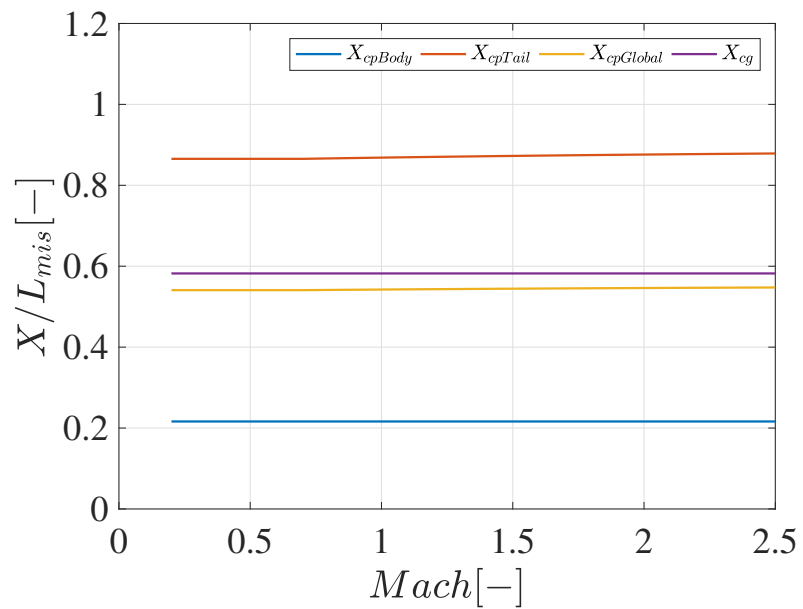


**Figure I.1:** Center of pressure position without flare.